

Full-length trimeric influenza virus hemagglutinin II membrane fusion protein and shorter constructs lacking the fusion peptide or transmembrane domain: Hyperthermostability of the full-length protein and the soluble ectodomain and fusion peptide make significant contributions to fusion of membrane vesicles[☆]



Punsisi U. Ratnayake, E.A. Prabodha Ekanayaka, Sweta S. Komanduru, David P. Weliky^{*}

Department of Chemistry, Michigan State University, East Lansing, MI 48824, United States

ARTICLE INFO

Article history:

Received 12 July 2015

and in revised form 17 August 2015

Accepted 18 August 2015

Available online 19 August 2015

Keywords:

Influenza virus
Membrane fusion
Hemagglutinin
Fusion peptide
Transmembrane domain

ABSTRACT

Influenza virus is a class I enveloped virus which is initially endocytosed into a host respiratory epithelial cell. Subsequent reduction of the pH to the 5–6 range triggers a structural change of the viral hemagglutinin II (HA2) protein, fusion of the viral and endosomal membranes, and release of the viral nucleocapsid into the cytoplasm. HA2 contains fusion peptide (FP), soluble ectodomain (SE), transmembrane (TM), and intraviral domains with respective lengths of ~25, ~160, ~25, and ~10 residues. The present work provides a straightforward protocol for producing and purifying mg quantities of full-length HA2 from expression in bacteria. Biophysical and structural comparisons are made between full-length HA2 and shorter constructs including SHA2 ≡ SE, FHA2 ≡ FP + SE, and SHA2-TM ≡ SE + TM constructs. The constructs are helical in detergent at pH 7.4 and the dominant trimer species. The proteins are highly thermostable in decylmaltoside detergent with $T_m > 90$ °C for HA2 with stabilization provided by the SE, FP, and TM domains. The proteins are likely in a trimer-of-hairpins structure, the final protein state during fusion. All constructs induce fusion of negatively-charged vesicles at pH 5.0 with much less fusion at pH 7.4. Attractive protein/vesicle electrostatics play a role in fusion, as the proteins are positively-charged at pH 5.0 and negatively-charged at pH 7.4 and the pH-dependence of fusion is reversed for positively-charged vesicles. Comparison of fusion between constructs supports significant contributions to fusion from the SE and the FP with little effect from the TM.

© 2015 Elsevier Inc. All rights reserved.

Abbreviations: Buffer A, 50 mM phosphate, 0.5% SRC, 50 mM sodium phosphate, and 300 mM NaCl at pH 8.0; Buffer B, 10 mM Tris-HCl, 0.17% DM, and 1 mM DTT at pH 7.4; Buffer C, 10 mM Tris-HCl, 0.10% SRC, and 1 mM DTT at pH 7.4; CD, circular dichroism; DM, decylmaltoside; DOTAP, 1,2-dioleoyl-3-trimethylammonium-propane (chloride salt); DTT, dithiothreitol; Endo, endodomain; FP, fusion peptide; HA, hemagglutinin; HA-cell, HA-expressing cell; HEPES, 4-(2-hydroxyethyl)-1-piperazineethanesulfonic acid; IB, inclusion body; IPTG, isopropyl β-D-1-thiogalactopyranoside; LB, Luria-Bertani; MES, 2-(*N*-morpholino)ethanesulfonic acid; *N*-NBD-DPPE, *N*-(7-nitro-2,1,3-benzoxadiazol-4-yl) (ammonium salt) dipalmitoylphosphatidylethanolamine; *N*-Rh-DPPE, *N*-(lissamine rhodamine B sulfonyl) (ammonium salt) dipalmitoylphosphatidylethanolamine; POPC, 1-palmitoyl-2-oleoyl-sn-glycero-3-phosphocholine; POPG, 1-palmitoyl-2-oleoyl-sn-glycero-3-[phospho-rac-(1-glycerol)] (sodium salt); RBC, red blood cell; RP, recombinant protein; SE, soluble ectodomain; SEC, size-exclusion chromatography; SRC, *N*-lauroylsarcosine; SSNMR, solid-state nuclear magnetic resonance; TM, transmembrane; Tris-HCl, tris(hydroxymethyl)aminomethane.

[☆] The research was supported by the National Institutes of Health grant R01 AI047153.

^{*} Corresponding author.

E-mail address: weliky@chemistry.msu.edu (D.P. Weliky).

1. Introduction

Influenza is a class I enveloped virus surrounded by a membrane obtained during budding from an infected host cell. The membrane contains hemagglutinin (HA) protein which assembles as three HA1 and three HA2 subunits with ~400 HA trimers per virion [1]. HA2 is a single-pass integral membrane protein with fusion peptide (FP), soluble ectodomain (SE), transmembrane (TM), and endodomain regions with respective lengths of ~25, 160, 25, and 10 residues (Fig. 1). The ectodomain is outside the virus as is the ~330-residue HA1 subunit. Infection of respiratory epithelial cells is initiated by binding of the HA1 subunits to cellular sialic acid receptors. The virus is then endocytosed and subsequent reduction of the endosomal pH to the 5–6 range leads to a large structural rearrangement of HA2 subunits followed by fusion (joining) of the viral and endosomal membranes. The timescale of fusion is several minutes [2]. To our knowledge, it isn't known whether influenza fuses

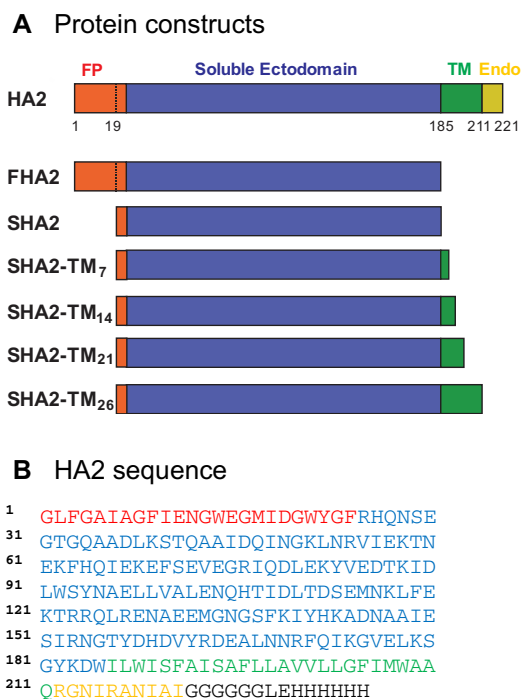


Fig. 1. Panel A displays a schematic of the HA2 constructs with domains colored: fusion peptide (FP), red; soluble ectodomain (SE), blue; transmembrane (TM) domain, green; and endodomain (Endo), yellow. The SHA2-TM₇, SHA2-TM₁₄, SHA2-TM₂₁, and SHA2-TM₂₆ constructs respectively include 7, 14, 21, and 26 residues of the transmembrane domain. Panel B displays the amino acid sequence of the HA2 construct with color-coding matching Panel A. The sequence has a non-native C-terminal region in black which includes a H₆ tag for affinity chromatography. (For interpretation of the references to color in this figure legend, the reader is referred to the web version of this article.)

initially with the membrane of the endosome or with the membrane of a vesicle in the interior of the endosome [3–5].

Much of our understanding of fusion of the influenza virus is based on fusion of HA-expressing cells with other cells or with vesicles [6–10]. Influenza fusion occurs within the endosome whereas in these studies, fusion is between the membrane of the virus or cell and the membrane of another cell or vesicle. To our knowledge, the significance of this difference, if any, is not known. There is likely some difference in fusion topology because the virus is enclosed within the endosomal body with which it fuses and successful fusion requires release of viral contents (nucleocapsid) outside of this body. In the model system, the fusing bodies do not enclose one another and successful fusion is considered to be mutual release of contents between them. This is more analogous to fusion of a virus with the plasma membrane which can occur for other viruses like HIV [11].

There is significant sequence conservation of HA2 across viral strains, particularly in the FP [12]. The FP and TM are important in fusion of influenza or HA-expressing cells with other cells or vesicles and are the only HA2 regions which are deeply inserted in the fused membrane [6,13–16]. Exogenous addition of many HA2 constructs to solutions of vesicles (often negatively-charged) leads to vesicle fusion with greater fusion at pH 5.0 than pH 7.4 [17–21]. Fusion is typically greater for a construct containing both the FP and the SE than for either the FP or SE alone. Fusion is impaired for the G1E mutant in the FP region which matches the effect of this mutant on HA-catalyzed cell/cell fusion. There is also leakage of small molecules out of the vesicles and the rates of leakage and fusion are comparable [19]. Leakage has also been observed in virus/vesicle fusion and is likely not problematic for intracellular influenza fusion so there probably isn't evolutionary bias against it [8]. Such bias is expected for other viruses which

fuse directly with the plasma membrane because leakage could disrupt cell homeostasis and result in cell death.

There is a crystal structure of the HA2 ectodomain (FP + SE) in its initial complex with HA1 [22]. Three HA2 molecules form a trimer in complex with three HA1 molecules. A structure of the SE without HA1 also shows three molecules each with hairpin structure with N-terminal regions (residues 38–105) forming a helical bundle followed by a 180° turn and C-terminal regions on the outside of the bundle and antiparallel to the N-terminal regions [23]. This is probably the final HA2 state in fusion. Although the FP and TM are not in the construct, the structure implies that they both on the same end of the hairpin which is opposite the hairpin turn.

There are also several structures of the monomeric FP in detergent-rich media with significant differences among these structures [24–26]. In particular, a peptide composed of the 20 N-terminal HA2 residues has (N-helix)-(open turn)-(C-helix) structure at pH 5 and (N-helix)-(open turn)-(C-coil) structure at pH 7. At pH 5, the structure is an “open boomerang” with an oblique angle between the N- and C-helices. In some contrast, a peptide composed of the 23 N-terminal HA2 residues has (N-helix)-(tight turn)-(C-helix) “closed hairpin” structure in detergent at both pH 5 and 7. The helices are antiparallel with close contact including hydrogen bonds between the N- and C-helices. The hydrophobic surfaces of the open and closed structures are also different and are located in the interhelical pocket (open structure) or on a shared face of the two helices (closed structure). These different hydrophobic surfaces are the basis for different models of membrane binding, either membrane insertion of the N-helix (open structure) or membrane surface location of the hydrophobic face (closed structure).

To our knowledge, neither peptide catalyzes fusion between detergent-rich micelles or bicelles but both peptides catalyze inter-vesicle fusion for peptide:lipid mole ratio of ~1:50 [27]. Fusion is moderately higher for the 23-residue relative to the 20-residue peptide and for pH 5 relative to pH 7. Fusion for both peptides at both pH's is difficult to understand based on the very different structures reported in detergent but is well-correlated to their structures in membrane. Both peptides adopt (N-helix)-(tight turn)-(C-helix) structure in membrane at both pH 5 and 7 [27–29]. The helices can either pack tightly in the closed structure or a little less tightly in a semi-closed structure. For both peptides at both pH's, there are significant populations of both structures with greater semi-closed population at pH 5. The moderate differences in vesicle fusion correlate well with moderate differences in hydrophobic surface areas, with greater surface area for the 23-residue relative to the 20-residue peptide and for the semi-closed relative to the closed structure.

The present work enhances our understanding of HA2-mediated fusion. Purified full-length HA2 is produced in mg quantities after expression in bacteria as well as the shorter constructs SHA2 (SE), FHA2 (FP + SE), and SHA2-TM (SE + TM). All constructs can form folded trimers in detergent. At pH 5.0, the constructs are positively-charged and induce significant fusion of negatively-charged vesicles whereas at pH 7.4, the constructs are negatively-charged and induce negligible fusion. The contribution of attractive protein-vesicle electrostatics is further supported by significant HA2-induced fusion of positively-charged vesicles at pH 7.4 with much less fusion at pH 5.0. Comparison of fusion among constructs reveals that the SE is the most important region for fusion with moderate effect of the FP and little effect of the TM.

2. Materials and methods

2.1. Constructs, bacterial culture, and protein expression

Fig. 1A displays a schematic of the HA2 constructs of the present study with color coding of different regions. Fig. 1B displays

the amino acid sequence of full-length HA2 (residues 1–221) with color coding matching Fig. 1A. The sequence corresponds to the X31 strain of influenza virus except that all native cysteines are mutated to other amino acid types, either serine (residue 137) or alanine (residues 144, 148, 195, 199, 210, 217, and 220). Non-native residues at the C-terminus are color-coded black in the sequence and include a H₆ tag for affinity chromatography and preceding G₆ to increase H₆ exposure during this chromatography.

Other constructs include FHA2 (residues 1–185) ≡ full ectodomain ≡ FP + SE, SHA2 (residues 20–185) ≡ primarily SE, and SHA2-TM₇, SHA2-TM₁₄, SHA2-TM₂₁, and SHA2-TM₂₆ ≡ SE + 7, 14, 21, and 26 TM residues, respectively. The term SHA2-TM refers to these latter four constructs. The amino acid sequences of all constructs are given in Fig. S1.

The DNA coding for each construct was inserted in a pUC57-Kan plasmid with codon-optimization for *Escherichia coli*. The sequence of the construct was then subcloned via the Nde1 and Xho1 restriction sites into a pet24a(+) plasmid that contained the Lac operon and kanamycin resistance. The DNA sequence of the HA2 insert is given in Fig. S2. The plasmid was transformed into *E. coli* cells, BL21(DE3) strain, followed by preparation of 1 mL stock cultures with 50% glycerol that were then stored at –80 °C. Culture growth was initiated by adding bacterial stock to a flask containing 50 mL LB broth and kanamycin antibiotic (50 mg/L). After growth overnight at 37 °C with stirring at 180 rpm, the culture was added to a baffled flask containing 1 L of fresh LB medium with kanamycin. After growth to OD₆₀₀ ≈ 0.5, recombinant protein (RP) expression was induced with addition of IPTG to 1 mM final concentration. Expression continued for five hours at 37 °C followed by centrifugation at 9000g for 10 min at 4 °C. The harvested cell pellet was stored at –20 °C.

2.2. RP solubilization and purification

For HA2 and SHA2-TM, much purer RP was obtained by first removing much of the native cellular material before performing RP solubilization. The separation began with sonication of ~5 g wet cell mass in 40 mL buffer (10 mM Na₂HPO₄, 2 mM KH₂PO₄, 140 mM NaCl, and 3 mM KCl at pH 7.4). Sonication conditions included 4 × 1 min rounds separated by 1 min rests. Each round was ~60 cycles consisting of 80% amplitude for 0.8 s followed by 0.2 s rest. After sonication, the insoluble material was pelleted by centrifugation (48000g for 20 min at 4 °C). Relative to whole cells, the pellet was enriched in RP both from the bacterial membrane and from inclusion bodies. There were two subsequent courses of sonication/centrifugation of the insoluble material.

For all RP's, solubilization was achieved by sonication in 40 mL of buffer A (50 mM phosphate, 0.5% *N*-lauroylsarcosine (SRC) detergent, 50 mM sodium phosphate, and 300 mM NaCl at pH 8.0) with 10 mM imidazole. Sonication of either the HA2- or SHA2-TM-enriched pellet resulted in a clear solution which was then stirred for one hour. No solid was visible after centrifugation which supports complete RP solubilization. RP separation was not used for SHA2 and FHA2 because purified yields of >10 mg/L culture were obtained from sonication of whole cells in buffer A with 10 mM imidazole followed by centrifugation and purification of the soluble lysate.

The purification procedure began with addition of 1 mL of Co²⁺ affinity resin to the ~40 mL solution containing RP. Binding of RP to the resin was achieved during one hour of agitation at ambient temperature. The RP-coated beads were separated by pouring the suspension through a fritted column. Weakly-bound proteins were removed from the beads by addition of buffer A containing 10 mM imidazole (0.75 mL, 3×). RP was then eluted from the beads by addition of buffer A containing 250 mM imidazole (0.50 mL, 4×). RP was quantitated using A₂₈₀ as well as the Bradford assay.

2.3. RP identification

The RP was first detected as a band at the expected MW in SDS-PAGE of the protein elution. Protein identity was further investigated by transfer to a nitrocellulose membrane for Western blotting with an anti-H₆ antibody. The membrane was incubated for one hour with 10 ml of TBST solution at pH 7.6 containing antibody and 5% (w/v) nonfat dry milk. The membrane was developed using SuperSignal West Pico chemiluminescent substrate.

RP identity was also investigated by subjecting the band from SDS-PAGE to trypsin digestion, sequencing the resultant peptides by tandem mass spectrometry, and matching with continuous regions of the RP sequence. Additional accurate mass analysis was done using reverse-phase HPLC coupled to a time-of-flight mass spectrometer (Waters, Xevo G2-S). Sample preparation included protein precipitation from the eluent using acetonitrile followed by centrifugation. The protein pellet was dissolved in formic acid and the solution was injected into the LC-MS instrument. Instrument parameters included a C18 analytical column and electrospray ionization in positive ion and continuum modes. The protein masses were derived from the spectrum using a maximum entropy algorithm.

2.4. Circular dichroism (CD)

Spectra were obtained with a Chirascan instrument (Applied Photophysics). Parameters included: (1) ~20 μM protein concentration; (2) 1 mm pathlength; (3) 260–190 nm spectral range with 0.5 nm wavelength increments and 1.5 s averaging time; and (4) summing of three scans. The final spectrum was the (protein + buffer) – (buffer only) difference. For each of the four constructs (SHA2, FHA2, SHA2-TM₂₆, and HA2), the “textbook” α helix shape of the CD spectrum was reproducible among replicate samples. There was some variability in the magnitude of the absolute molar ellipticity among replicate samples, probably because of A₂₈₀ measurement error with the NanoDrop instrument. Comparative spectra of the four constructs at ambient temperature were obtained by: (1) simultaneous purification and sample preparation; and (2) successive spectral acquisition within a single day. This approach resulted in similar molar ellipticities among the constructs. For each construct, a different sample was prepared for which spectra were obtained at a series of increasing temperatures. These samples were prepared on different days and there was greater variability of absolute molar ellipticities between samples.

2.5. Detergent exchange and refolding

A large fraction of α helical structure is observed in the high-resolution structure of the soluble ectodomain and in structures of the FP fragment in membrane and detergent environments. The TM region is also expected to be an α helix. The degree of folding of a protein was therefore assessed by the far-UV CD spectrum, in particular the characteristic signatures of α helical structure, minima at 208 and 222 nm with |θ₂₂₂| > 10⁴ degrees-cm²-dmol⁻¹-residue⁻¹. CD spectra could not be obtained from the RP eluent because of ultraviolet absorption by imidazole and SRC detergent. Imidazole was removed and SRC exchanged for decylmaltoside (DM) detergent by dialysis against buffer B (10 mM Tris-HCl, 0.17% DM, and 1 mM DTT at pH 7.4). This dialysis and subsequent dialyses were done at 4 °C over two days with four buffer changes. Precipitation was not observed during dialyses. The CD spectra supported folding for SHA2 and FHA2 but not for HA2 and SHA2-TM. The latter eluents were therefore subjected to a refolding protocol in which eluent was added to twofold excess ice-cold buffer (10 mM Tris-HCl, 0.17% DM, 2 mM EDTA, and 1 M

L-arginine at pH 8.0) [30,31]. After overnight agitation at 4 °C, the arginine and EDTA were removed by dialysis against buffer B.

2.6. Cross-linking

Protein in buffer B was dialyzed into buffer containing 20 mM HEPES and either 0.17% DM or 0.1% SRC at pH 7.4. Cross-linking between lysine $-NH_2$ groups of the RP molecules was done with bis(sulfosuccinimidyl) suberate. Cross-linking was done with [RP] = 0.5 mg/mL and with 50-fold molar excess cross-linking agent. The reaction was done at room temperature for one hour and then quenched by adding Tris-HCl at pH 6.8 with final [Tris-HCl] = 50 mM. The oligomer sizes were analyzed by SDS-PAGE.

2.7. Size-exclusion chromatography (SEC)

The SEC columns require [NaCl] \geq 150 mM in the running buffer to inhibit electrostatic interaction between the protein and the column. The protein solution in buffer B was therefore dialyzed against buffer B with 150 mM NaCl or against buffer C (10 mM Tris-HCl, 0.10% SRC detergent, and 1 mM DTT at pH 7.4) with 150 mM NaCl. The chromatography was done with a DuoFlow Pathfinder 20 instrument (Bio-Rad) with Tricorn Superdex 200 semi-preparative column (General Electric). The column was equilibrated with dialysis buffer before each run. Parameters included 0.8 mg protein/mL loading concentration, 0.3 mL/min flow rate, and A_{280} detection.

2.8. Protein-induced vesicle fusion

Lipid was dissolved in chloroform followed by chloroform removal with nitrogen gas and vacuum pumping. The film was homogenized by freeze-thaw cycles in \sim 1 mL buffer and extruded through 100 nm diameter pores to form unilamellar vesicles. The buffer contained 5 mM HEPES/10 mM MES at either pH 5.0 or 7.4. Fluorescently labeled vesicles were similarly prepared except that the mixture also contained 2 mol% of the fluorescent lipid N-NBD-PE and 2 mol% of the quenching lipid N-Rh-PE. Labeled and unlabeled vesicles were mixed in 1:9 ratio with total [lipid] \approx 150 μ M. Fluorescence of the stirring vesicle solution was measured at 37 °C with 467 nm excitation, 530 nm detection, and 1 s time increment. After measurement of the baseline fluorescence F_0 , a protein aliquot from stock was added and marked time $t = 0$. Vesicle fusion was reflected in the increased fluorescence

$\Delta F(t) = F(t) - F_0$ due to longer distances between fluorescent and quenching lipids in a fused (labeled + unlabeled) vesicle relative to the initial labeled vesicle. The dead-time in the assay was \sim 5 s and asymptotic fluorescence (ΔF_f) was usually reached by \sim 600 s. The maximum fluorescence change (ΔF_{max}) was detected after addition of 12 μ L 10% Triton X-100 which solubilized the vesicles. Percent fusion was $M(t) = [\Delta F(t)/\Delta F_{max}] \times 100$. Comparison among assay replicates showed $\delta(M_f)/M_f \approx 0.02$. The protein stock contained 40 μ M protein in 10 mM Tris-HCl at pH 7.4 with 1 mM DTT and either 0.17% DM (HA2 and SHA2-TM) or 0.10% SRC (FHA2 and SHA2). For these detergent choices, the trimer is the dominant protein oligomeric species. No fusion was detected after addition of either detergent solution without protein.

3. Results

3.1. RP solubilization and purification

The first approach was sonication of the cell mass in Buffer A containing 0.5% SRC detergent followed by centrifugation and Co^{2+} affinity chromatography of the supernatant. For SHA2 and FHA2, SDS-PAGE of the purification eluent showed highly pure RP with respective yields of \sim 15 and \sim 10 mg/L culture (Fig. 2). RP identity was supported by clear bands in the anti- H_6 Western blot. In some contrast, for SHA2-TM or full-length HA2, there were significant impurities after purification. Low expression was likely not the problem because analysis of solid-state NMR spectra of RP-expressing cells has always shown \geq 100 mg RP/L culture including for RP \equiv FHA2 [32].

In our experience, Co^{2+} affinity chromatography can be compromised with too small a RP:native protein ratio, likely because the native protein rather than RP binds to the Co^{2+} sites. Many native proteins are soluble in PBS whereas there is low solubility for SHA2-TM and HA2. Separation based on this solubility difference was done by sonication of the cell mass in PBS followed by centrifugation and discarding the supernatant enriched in cell protein. The procedure was repeated three times and followed by complete solubilization of the RP-enriched pellet in buffer containing SRC, and subsequent Co^{2+} -affinity chromatography. This protocol resulted in high-purity SHA2-TM and HA2 with purified yield of \sim 2 mg HA2/L culture (Fig. 2). The proteins are primarily monomeric in SDS-PAGE with a small fraction of dimer.

Different solubilizing agents such as 8 M urea and 6 M GuHCl were also tried but the highest yields were obtained with 0.5%

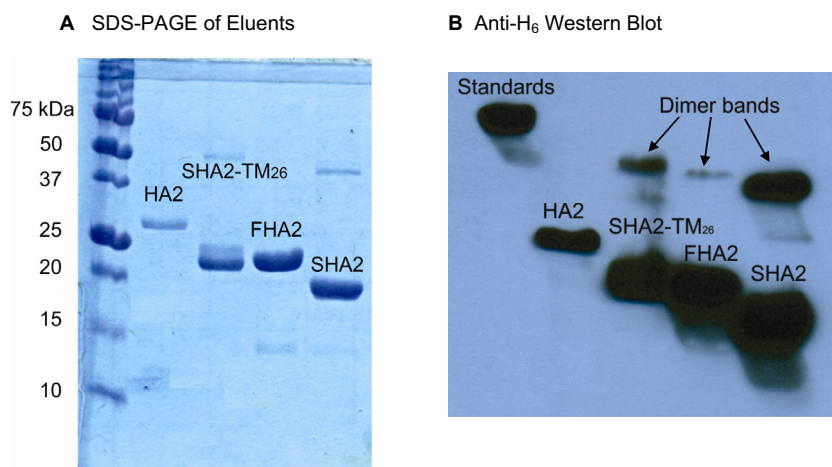


Fig. 2. Panel A displays SDS-PAGE of the purification eluents and panel B is the corresponding anti- H_6 Western blot. The expected MW's are: HA2, 26.7 kDa; SHA2-TM₂₆, 23.7 kDa; FHA2, 22.4 kDa, and SHA2, 20.4 kDa. Dominant monomer and minor dimer bands are observed where the latter is evidenced by binding to the anti- H_6 antibody and by qualitatively similar dimer:monomer intensity ratios in SDS-PAGE and Western blots.

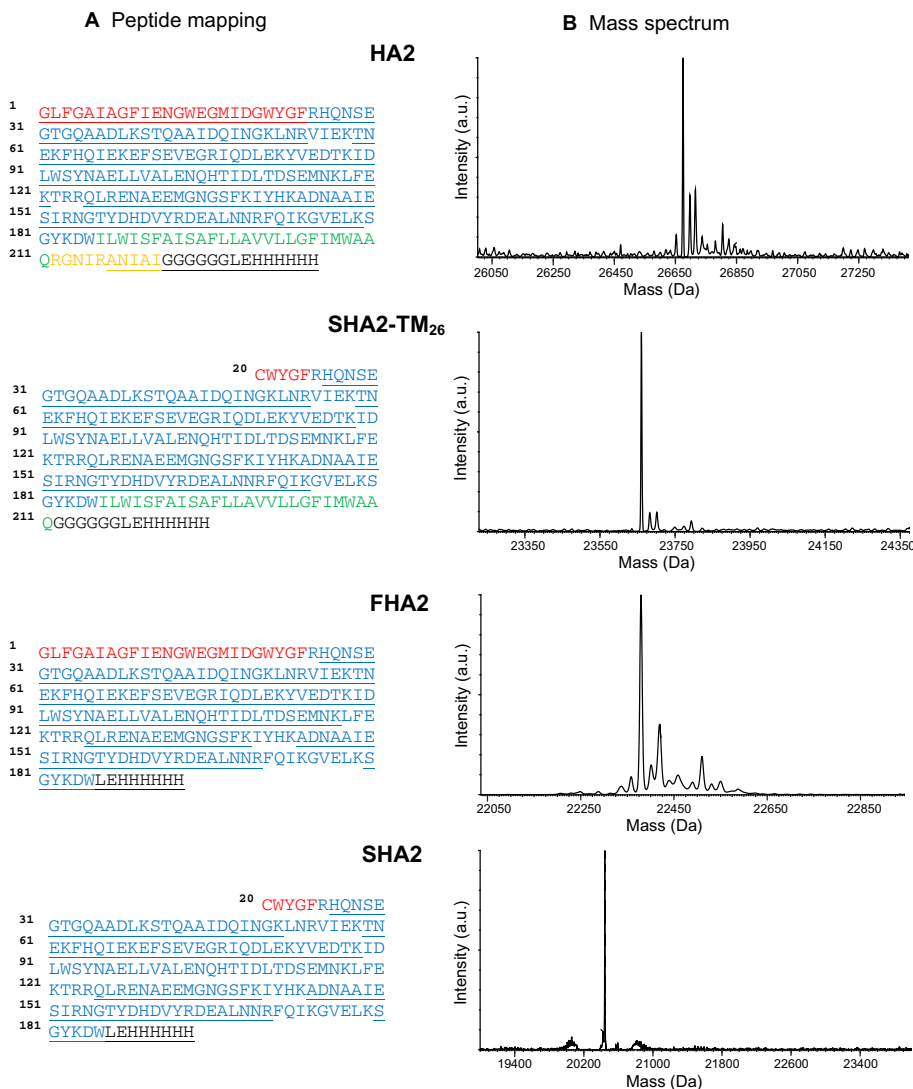


Fig. 3. (A) Peptide mapping via trypsin digestion and mass spectrometry; and (B) analysis of liquid chromatography–electrospray ionization mass spectra. The mapping in panel A was done for the most intense monomer band of the SDS–PAGE of the purification eluent (Fig. 2). The underlined regions of a sequence correspond to detected peptides and the percent sequence coverages are: HA2, 81%; SHA2-TM₂₆, 55%; FHA2, 77%; and SHA2, 65%. The color coding of the sequences matches Fig. 1. The experimental peak masses in panel B and expected masses are: HA2, 26,678 and 26,676 Da; SHA2-TM₂₆, 23,663 and 23,663 Da; FHA2, 22,379 and 22,378 Da; and SHA2, 20,444 and 20,444 Da. The primary mass spectra are presented in Fig. S5.

SRC (Fig. S3). Higher purified yields were obtained for SHA2-TM with a G₆LEH₆ C-terminal tag than with a LEH₆ tag (Fig. S4). Inclusion of the G₆ spacer may result in greater H₆ exposure and consequent better RP binding to the Co²⁺ resin.

Solubilization and purification of HA2 was also tried using 0.17% DM, 0.10% dodecylmaltoside, or 0.10% dodecylphosphocholine detergents. There was poorer solubilization as well as much lower final purities and yields with these detergents than with 0.5% SRC. Sodium dodecyl sulfate detergent had previously been successfully used for solubilization and purification of the related “Fgp41” full ectodomain construct of the HIV gp41 membrane fusion protein [33]. There was better solubilization of Fgp41 with SDS than with SRC but SDS is poorly exchangeable and we have not yet tried SDS with the HA2 constructs.

3.2. RP confirmation by mass spectrometry

The SDS–PAGE band thought to be RP was digested with trypsin and the fragment peptides were sequenced by tandem mass

spectrometry (Fig. 3A). For all RP’s, there is good matching between the peptides and continuous regions of the RP sequence. It is particularly significant that full-length HA2 has 81% sequence coverage including the FP and endodomain regions. Additional confirmation was obtained from LC–MS of the RP eluents with each experimental mass within 3 Da (0.01%) of the expected mass (Fig. 3B).

3.3. Hyperthermostable α helical structure

Fig. 4A displays CD spectra of the HA2 constructs in 0.17% DM detergent at pH 7.4. The spectra of the four constructs are similar and have the profile characteristic of proteins with high α helical content including minima at 208 and 222 nm. The spectra have similar appearance in 0.30% DM or at pH 9.0 (Fig. S6). The proteins visibly aggregate at either pH 5.0 and 3.0 so spectra were not obtained at these lower pH values. A \sim 65% α helical content is estimated from the experimental $[\theta_{222}] \approx 2 \times 10^4$ degrees-cm² dmol⁻¹-residue⁻¹ and agrees semi-quantitatively with \sim 60% α helical content calculated for HA2 based on the high-resolution

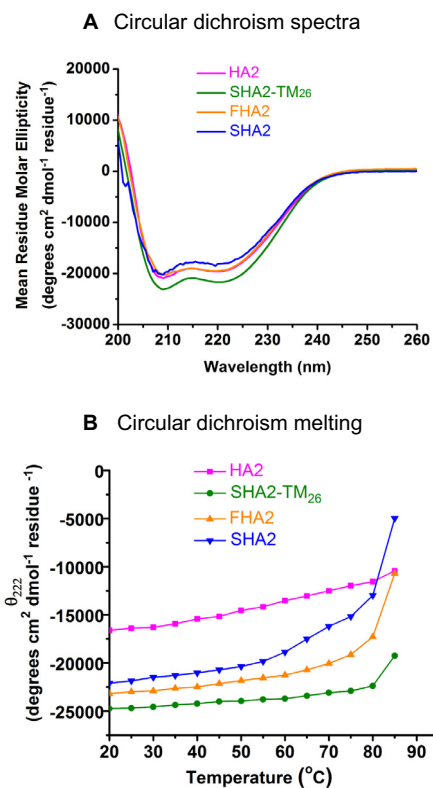


Fig. 4. Circular dichroism (A) spectra and (B) melts of samples containing $\sim 20 \mu\text{M}$ protein in buffer with 10 mM Tris-HCl, 0.17% DM detergent, and 1 mM DTT at pH 7.4. The panel A spectra were obtained at ambient temperature and the panel B melting is for the mean-residue molar ellipticity at 222 nm.

structures of FP and SE fragments and the predicted α helical structure in the ~ 25 -residue TM domain [23,25,27].

Spectra were obtained for a series of temperatures between 20 and 85 °C (Fig. S7) and the $|\theta_{222}|$ were plotted vs temperature (Fig. 4B). SHA2 exhibits a small linear decrease in $|\theta_{222}|$ between 20 and 55 °C, greater linear decrease between 55 and 75 °C, and even larger decrease between 75 and 85 °C. This multi-step behavior may be due to the aggregation of SHA2 in DM and greater description is provided in the Section 4. FHA2, SHA2-TM₂₆, and HA2 behave more simply and exhibit small linear decreases in $|\theta_{222}|$ between 20 °C and ~ 75 , 80, and 85 °C, respectively. For FHA2 and SHA2-TM₂₆, there are more significant decreases approaching 85 °C which indicate onset of unfolding. For FHA2, the estimated $T_m \approx 85$ °C based on $|\theta_{222}(85 \text{ °C})|/|\theta_{222}(20 \text{ °C})| \approx 1/2$ and for SHA2-TM₂₆, the $T_m > 85$ °C. There is no indication of unfolding of full-length HA2 for temperatures ≤ 85 °C, so HA2 appears to adopt a hyperthermostable structure which is likely the final HA2 state in HA-mediated fusion. Overall, the CD-detected melting in DM support a thermostable SE in HA2 and the ordering of stability FHA2 < SHA2-TM₂₆ < HA2 supports additional stabilization associated with the FP and TM.

3.4. Trimers and higher-order oligomers at pH 7.4

For [protein] = 0.8 mg/mL at 4 °C, all HA2 constructs remain soluble in pH 7.4 buffer that contains either 0.17% DM or 0.10% SRC detergent, e.g. after one day, there were no visible precipitates after centrifugation of these solutions. The protein oligomeric states were investigated with these two detergent conditions.

The cross-linking experiments used [protein] = 0.8 mg/mL and with either DM or SRC, the protein:detergent mole ratio is $\sim 1:110$. Although the loading [protein] = 0.8 mg/mL in the SEC,

the running concentration is about ten-fold lower, so that the protein:detergent mole ratio is $\sim 1:1100$. The 0.17% DM concentration is about $2 \times \text{CMC}$ and the aggregation number is ~ 70 so that protein:micelle ratio is $\sim 1:1.6$ in cross-linking and $\sim 1:16$ in SEC. Although the 0.10% SRC concentration is below its CMC, the aggregation number is ~ 2 so the SRC “micelle” is just a dimer and there isn’t significant difference in detergent state below vs above the CMC.

Fig. 5A displays SDS-PAGE of HA2 constructs after one hour of chemical cross-linking. For protein in either detergent, there is typically a band in the 60–80 kDa range that likely corresponds to a trimer. For SHA2 and FHA2 in DM, there are also bands at higher MW’s that correspond to larger oligomers and for SHA2, a significant fraction of these oligomers are so massive that they don’t migrate in SDS-PAGE. There is only a small fraction of monomer protein with significant bound detergent mass, but this mass is not apparent in the SDS-PAGE because of SDS-induced unfolding of proteins, including standards, and SDS binding to the unfolded proteins and replacement of the bound DM or SRC in the HA2 proteins. The MW determination by SDS-PAGE via comparison with the protein standards therefore results in protein-only rather than protein + SDS masses.

SEC was done with folded non-cross-linked HA2 proteins which migrate with bound detergent whereas the soluble protein standards do not migrate with detergent. The MW’s determined by SEC are therefore for the HA2 + detergent complexes and include significant contributions from both protein and detergent masses. The SEC of all constructs in SRC shows a dominant oligomeric species with $\text{MW}_{\text{Prot+Det}} \approx 200$ kDa (Fig. 5B). This is also the dominant species for HA2 and SHA2-TM₂₆ in DM whereas the dominant species for FHA2 and SHA2 are larger with respective $\text{MW}_{\text{Prot+Det}}$ of ~ 400 kDa and ≥ 2 MDa with most SHA2 in the column void volume. For all constructs in DM, there is also a small population with $\text{MW}_{\text{Prot+Det}} \approx 50$ kDa. Fig. S9 displays the SEC of the MW standards and Fig. S10 displays a replicate SEC in DM for which there is a less sloped baseline.

The ~ 200 kDa species and ~ 50 kDa species in SEC are respectively assigned to protein trimer and monomer. These assignments are based in part on correlation to the cross-linking data showing major trimer and minor monomer species. The larger MW species in the SEC of FHA2 and SHA2 in DM are also consistent with the cross-linking data. The Section 4 describes additional support for these assignments by correlations with earlier studies of HA2 and HIV gp41 constructs. All constructs form visible aggregates at pH 5.0 in 0.17% DM. In addition, SHA2 forms aggregates at pH 7.4 in the absence of detergent.

3.5. Vesicle fusion

The HA2 fusion activities were probed by monitoring mixing of lipids between vesicles after addition of an aliquot of protein stock. The pH of the vesicle solution was either 7.4 or 5.0 with the latter pH closer to the 5–6 range of influenza virus fusion with endosomes. Fig. 6A displays fusion at pH 5.0 of vesicles containing 20 mol% negatively-charged lipid. All constructs induce significant and comparable rates and extents of vesicle fusion with increased extents for constructs that include the FP, e.g. HA2 vs SHA2-TM₂₆ and FHA2 vs SHA2. There is typical $\pm 1\%$ variation in fusion extents among assay replicates so the extents for HA2 and FHA2 are comparable and the extents for SHA2-TM₂₆ and SHA2 are comparable. Thus, there isn’t a significant effect of inclusion of the TM- or TM+ endo-domains and this is also evidenced by comparable fusion for SHA2-TM constructs with different length segments of the TM domain (Fig. S11B).

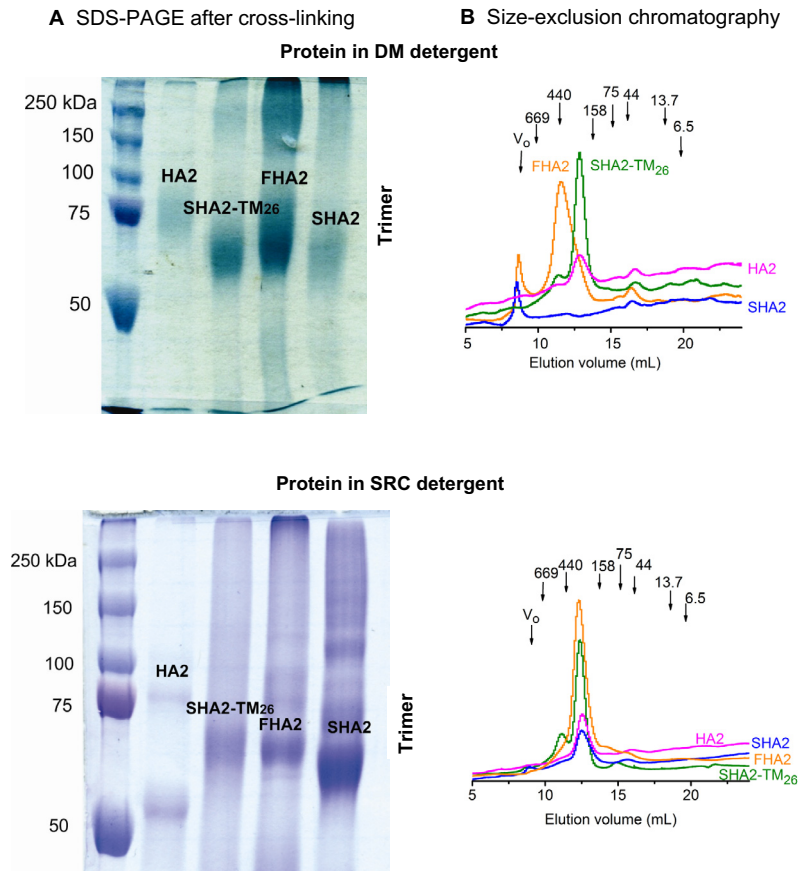


Fig. 5. (A) SDS-PAGE after chemical cross-linking and (B) SEC of the proteins in the absence of cross-linking. Solutions contained either (top) 0.17% DM or (bottom) 0.10% SRC detergent at pH 7.4. Cross-linking was done with pure proteins (Fig. 2) using bis(sulfosuccinimidyl) suberate and the displayed SDS-PAGE are 8% gels with band diffuseness at low MW's. The trimer region is marked. SEC was done with A_{280} detection and ~ 0.8 mg protein/mL loading. The vertical arrows in the plots mark the elution times of the MW standards with $V_0 \equiv$ column void volume. The SEC of the MW standards is provided in Fig. S7. A fraction of protein molecules are typically in oligomeric states larger than a trimer as evidenced by diffuse high MW intensity in SDS-PAGE and by A_{280} intensity at shorter SEC elution times.

The typical fusion rate is estimated to be $\sim 200 \text{ s}^{-1}$ based on typical achievement of at least half the final fusion extent during the ~ 5 s dead-time of the assay. Dose dependence is observed with significant fusion by FHA2 for protein:lipid = 1:1120 (Figs. 6B and S11A). This corresponds to ~ 15 trimers per 100 nm diameter vesicle (assuming quantitative binding) which is much smaller than the typical number of HA trimers per virion (~ 400).

There is little fusion of negatively-charged vesicles at pH 7.4 (Fig. S11C). One reason for this pH-dependence is attractive vs repulsive protein/vesicle electrostatic energies at pH 5.0 and 7.4, respectively, corresponding to the protein charges of $\sim +8$ and ~ -9 . This electrostatic contribution is also evident in the reversal of the pH-dependence of vesicle fusion for positively-charged vesicles (Fig. 6C). The fusion extent of positively-charged vesicles at pH 7.4 appears to be significantly larger than the fusion of negatively-charged vesicles at pH 5.0. For HA2 in 0.17% DM detergent, the major biophysical difference between pH 7.4 vs 5.0 is predominant trimer vs larger (likely multiple trimer) species. There may be a similar pH-dependent difference in oligomeric state in membrane that correlates to the different fusion extents.

HA2-induced fusion is also compared for neutral PC-only and negatively-charged PC:PG (4:1) vesicles (Fig. S11D). At 50 s after HA2 addition, there is at least twice the fusion of negatively-charged vesicles relative to neutral vesicles at pH 5.0 with little fusion of either vesicle-type at pH 7.4 [21]. These observations are consistent with HA2 binding to vesicles in descending order PC:PG (pH 5.0) > PC (pH 5.0) > PC (pH 7.4) > PC:PG (pH 7.4) with respective estimated $[\text{protein}]_{\text{bound}}/[\text{protein}]_{\text{free}}$ ratios of ~ 80 , 3, 0.5, and 0. The first three values are calculated using: (1) the

experimental binding constants to PC and PC:PG vesicles for the positively-charged HA3fp20 fusion peptide; and (2) [outer-leaflet lipid] $\approx 8 \times 10^{-5} \text{ M}$ in our vesicle fusion assays [34]. The HA3fp20 binding constants are used because to our knowledge, there aren't yet constants for larger HA2 constructs. Negligible HA2 binding to PC:PG vesicles at pH 7.4 is based on repulsive HA2/vesicle electrostatic energy.

Solution transparency was retained after protein addition for PC:PG vesicles at pH 5.0 and 7.4 and for PC vesicles at pH 7.4. In some contrast, the PC vesicle solution at pH 5.0 became cloudy after addition of protein. We previously observed that HA2 constructs aggregate at pH 5.0 but not 7.4 and we attribute the cloudiness to aggregation of unbound protein.

4. Discussion

4.1. Significant findings

The present paper describes production of mg quantities of purified full-length HA2 as well as shorter HA2 constructs via expression in *E. coli* without a large solubility tag. Folding of the proteins in detergent at pH 7.4 was evidenced by CD spectra consistent with helical structure and by predominant trimer species evidenced by cross-linking and SEC. The proteins are highly-thermostable in DM detergent with $T_m \approx 85^\circ \text{C}$ for FHA2 and $T_m > 90^\circ \text{C}$ for HA2 with major stabilization provided by the SE and additional stabilization from the FP and TM domains. The proteins efficiently fused negatively-charged vesicles at pH 5.0 but not

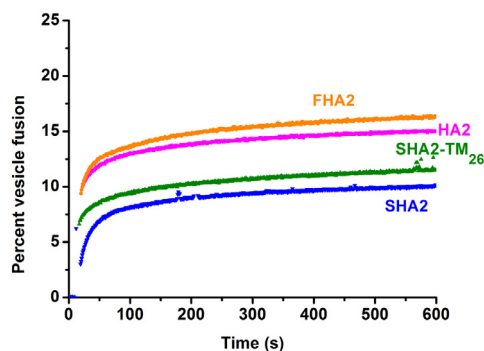
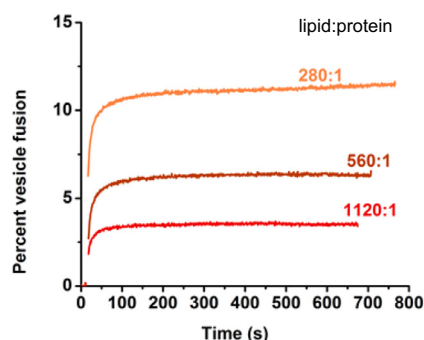
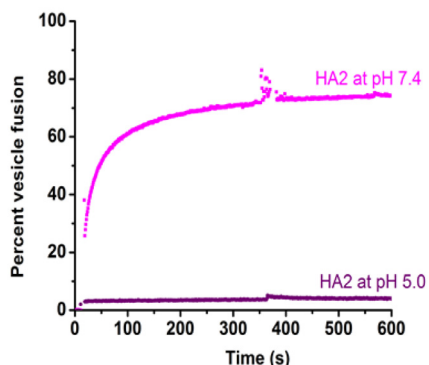
A Fusion of negatively-charged vesicles at pH 5.0**B** Dose response for FHA2**C** Fusion of positively-charged vesicles

Fig. 6. Protein-induced fusion of (A, B) negatively-charged vesicles at pH 5.0 and (C) positively-charged vesicles at pH 5.0 and pH 7.4. The protein:lipid mole ratio = 1:280 in panels A and C and is displayed for each trace in panel B. The vesicle composition is (A, B) POPC:POPG (4:1) and (C) POPC:DOTAP (4:1). For each trace, protein is added a few seconds before the first displayed point. There is typically $\pm 1\%$ variation in final extent of vesicle fusion among replicate assays and no fusion is observed with addition of detergent solution without protein.

pH 7.4 which corresponding positive and negative protein charges, respectively. The role of protein/vesicle electrostatic energy in vesicle fusion was further evidenced by much greater fusion of positively-charged vesicles at pH 7.4 than pH 5.0. Comparison between HA2 constructs showed a moderate enhancement of fusion with inclusion of the FP and little effect by inclusion of the TM. Efficient vesicle fusion is evidenced by its requirement of fewer than 15 HA2 trimers per vesicle which is lower by at least a factor of 10 from the number of HA2 trimers in the viral envelope.

4.2. Full-length HA2 purified from *E. coli*

To our knowledge, this is the first report of mg purified quantities from *E. coli* of full-length HA2 without a large

N-terminal solubility tag. Our accomplishment compares favorably with an earlier report (also reproduced in our laboratory) of a maltose-binding protein-HA2 construct that could be purified in mg quantities from *E. coli* but for which little HA2 was subsequently recovered after attempted cleavage of the maltose-binding protein [30]. Key points of our approach included: (1) removal of soluble *E. coli* proteins from the cell pellet prior to solubilization of the remaining proteins with SRC; and (2) a G_6LEH_6 rather than a LEH_6 tag to increase exposure of the H_6 region during affinity purification. The purified FHA2 yield of the present study is ~ 10 mg/L culture and is compared with >100 mg/L expression of FHA2. There is probably lower expression of full-length HA2 which includes the TM and corresponding lower purified yield of ~ 2 mg/L (Fig. 2). Although these yields are good for a non-bacterial membrane protein expressed in *E. coli*, there are $>90\%$ losses during solubilization and purification. The purification losses have previously been noted for FHA2 using SDS-PAGE with lanes for the soluble cell lysate and for washes and elutions from the Co^{2+} -affinity column with bound protein [31]. The lysate and wash lanes are similar with a band corresponding to FHA2 as well as bands with significant intensity corresponding to higher MW proteins. This supports some loss of FHA2 during the column washes. The eluent lane shows a dominant FHA2 band which is ~ 3 times more intense than the FHA2 band in the lysate. However, the eluent volume is ~ 10 times smaller than the lysate volume which also supports an overall loss of FHA2 during purification.

4.3. Dominant thermostable trimer supported by earlier biophysical studies

To our knowledge, the present study is the first to produce and study the full-length HA2, $SHA2 \equiv SE$, and $SHA2-TM_{26} \equiv SE + TM$ proteins. $FHA2 \equiv FP + SE$ has been previously studied as has the construct “F185” \equiv FLAG + FHA2 where FLAG \equiv DYKDDDDK [35]. Because of the 8-residue non-native hydrophilic FLAG tag, F185 is soluble at pH 7.0 in the absence of detergent and cross-linking and SEC shows that F185 forms a dominant trimer species. The major SEC peak of F185 reflects migration of protein-only and the mass agrees quantitatively with the expected value of a protein trimer. The CD spectrum of F185 in the absence of detergent is similar to our CD spectrum of FHA2 in detergent in Fig. 4A and the $[\theta_{222}]$ values correspond to $\sim 65\%$ α helical structure which is close to the $\sim 60\%$ value calculated using the high-resolution structure of the FP and the structure of a large region of the SE. In addition, the $[\theta_{222}]$ vs temperature for both constructs have sigmoidal shape with $T_m \approx 85$ °C. These good correlations between F185 and FHA2 support dominant trimers of our HA2 constructs with thermostable SE hairpin structure.

The major peaks in our SEC's are typically at ~ 200 kDa which is similar to the mass previously observed in the SEC of FHA2 in Brij-35 non-ionic detergent [35]. We assigned this peak to a protein trimer with ~ 80 kDa protein and ~ 120 kDa detergent contributions. This assignment is consistent with an earlier study on a MBP + HA2 construct that supported a dominant trimer species with hairpin HA2 SE structure based on analytical ultracentrifugation, electron microscopy, antibody-binding, and cross-linking data [30]. The MBP + HA2 had been solubilized at neutral pH in non-ionic detergents which included 0.17% DM which is used in our study. The major SEC peak for MBP + HA2 was at ~ 350 kDa with respective protein trimer and detergent mass contributions of ~ 200 and ~ 150 kDa. MBP is very soluble so it is reasonable that most of the detergent binds to HA2. It is therefore reasonable that similar detergent masses bind to trimeric MBP + HA2 and to trimeric HA2.

There is also semi-quantitative agreement between our SEC and the published SEC in non-ionic detergent of an ectodomain + TM construct of the HIV gp41 membrane fusion protein [36].

The HIV construct is functionally and structurally homologous to HA2. The gp41 SEC had a peak at ~ 180 kDa that was assigned to a protein trimer with respective protein and detergent mass contributions of ~ 60 and ~ 120 kDa.

4.4. SHA2 aggregation in DM

The FHA2 CD data in DM detergent at pH 7.4 is compared with a previous study in which the FHA2 was solubilized in 0.14 M NaF at pH 7.4 [21]. At ambient temperature, the CD-derived $[\theta_{222}]$ in NaF is about half that in DM. The $[\theta_{222}]$ vs temperature are different in NaF and DM with the NaF data resembling those of SHA2 in DM (Fig. 4B). There was a large decrease in $[\theta_{222}]$ between 55 and 65 °C, followed by leveling, and then a second large decrease between 75 and 85 °C. This behavior differs from the single sigmoidal curve for FHA2 in DM with $T_m \approx 85$ °C. For our SEC in DM, SHA2 forms large (>2 MDa) aggregates which is different from the other three constructs which are not aggregated (Fig. 5B). There was no SEC characterization of FHA2 in the earlier study but we propose that this protein was also aggregated which is reflected in the $[\theta_{222}]$ vs temperature. For SHA2 in DM and FHA2 in NaF, we propose that the 55–65 °C component corresponds to dissociation of the protein aggregates and the 75–85 °C component corresponds to unfolding of the SE. The latter assignment is consistent with the T_m of FHA2 in DM for which large aggregates are not formed.

4.5. Viral fusion overview

Influenza fusion occurs within endosomes which themselves are undergoing morphological and chemical changes in time [3]. Following initial endocytosis, the early endosome forms in ~ 5 min and is characterized by: (1) enlargement due to fusion with other endocytic vesicles; (2) pH reduced to ~ 6.2 ; and (3) migration from the plasma membrane towards the nucleus [2]. The late endosome forms in the next ~ 3 min and is characterized by: (1) creation of vesicles within the endosomal lumen; and (2) further lowering of pH to ~ 5.5 . The late endosome may then fuse with lysosomes which contains hydrolase enzymes that degrade proteins and whose pH < 5 . The membrane compositions of both the endosome and interior vesicles are different from one another and change during these maturation steps in a manner correlated to use of the endosomal pathway to transport cholesterol in and out of the cell [37,38].

The fusion trigger pH of 5–6 for influenza supports fusion within the late endosome which is formed after the early endosome and prior to the endosome–lysosome hybrid. To our knowledge, it isn't clear whether the virus fuses first with the outer membrane of the late endosome or with the membrane of one of the vesicles within the endosomal lumen. For the former circumstance, the viral nucleocapsid is released directly into the cytosol close to the nucleus whereas in the latter circumstance, nucleocapsid release into the cytosol requires an additional event such as back-fusion with the endosomal membrane. The influenza virus can fuse with membranes with a variety of compositions so fusion is probably not influenced by composition differences between outer vs interior endosomal membranes or by differences at different stages of endosome maturation [8].

To our knowledge, there has been little detailed study of virus/endosome fusion. There have been some studies of virus/vesicle fusion but most detailed studies have examined fusion between cells expressing HA (HA-cells) and cells containing sialic acid but not HA (often Red Blood Cells – RBC's) [7,9,10]. One dye (typically small-molecule) is incorporated in the RBC membrane and a different dye incorporated into the RBC cytoplasm. Fusion is triggered by lowered pH. Subsequent intercellular lipid mixing is quantitated

by the percentage of HA-cells containing membrane dye while intercellular contents mixing is quantitated by the percentage cells containing cytoplasmic dye. Lipid mixing without contents mixing is often considered evidence for arrest at a hemifusion intermediate state. In cases in which neither lipid nor contents mixing are observed with lowered pH, a small molecule like chlorpromazine is sometimes added and becomes membrane-incorporated. Subsequent lipid and contents mixing has been interpreted to mean that HA alone had induced "hemifusion with restricted lipid movement" where the restriction prevented movement of the RBC membrane dye into the HA-cell membrane [10].

Although cell/cell fusion shares common features with virus/endosome fusion, one topological difference is initial physical separation of the two cells vs initial enclosure of the virus within the endosome. In addition, unlike cell/cell fusion, there may be significant contents leakage during virus/endosome fusion. Leakage has been observed in virus/vesicle fusion and leakage in intracellular virus/endosome fusion probably doesn't hurt cell viability so there isn't evolutionary selection against it [8].

4.6. Common fusion features

The present study describes HA2-catalyzed vesicle fusion using stock solutions with predominant folded hairpin trimer species. Such protein characterization has typically not been done in vesicle fusion studies but is very useful because it provides information about the likely protein structure during initial interaction with the membrane (Fig. 7). This may also be the fusogenic structure.

Unlike vesicle/vesicle fusion for which HA2 initially has hairpin structure, virus/endosome and HA-cell/RBC fusion initially have HA2 in non-hairpin structure in complex with HA1. Upon pH reduction, HA1 dissociates and HA2 folds into the final hairpin state. It has often been assumed that some of the free energy released upon folding (ΔG_{fold}) provides activation energy for fusion ($\Delta G_{fusion}^{\ddagger}$) [7,39]. For vesicle/vesicle fusion, HA2 always has hairpin structure so $\Delta G_{fold} \approx 0$ and $\Delta G_{fusion}^{\ddagger}$ would be influenced by membrane interactions of the hairpin SE and the FP.

There is evidence that the HA2 hairpin is a fusogenic structure in cell/RBC fusion. In particular, FHA2 and truncated FHA2_{trunc} (residues 1–127) catalyze cell/RBC fusion including the steps of intercellular lipid mixing and small-molecule contents mixing [21,40]. Both constructs are presumed to be in the final hairpin state. Large pores are not formed but this may be due to no TM in either FHA2 construct. The TM is required for formation of large pores in HA-cell/RBC fusion [7]. There are many correlations between HA-cell/RBC fusion and FHA2-catalyzed cell/RBC fusion including: (1) low pH requirement; (2) reduction in fusion with the G1E and V173E mutations which are respectively in the FP and SE domains; (3) reduction in fusion with addition of lysophosphatidylcholine detergent with positive curvature; (4) reduction in fusion at 4 °C and fusion recovery upon return to 37 °C; and (5) increased fusion under some circumstances with addition of chlorpromazine dye [10]. All these correlations are consistent with similar mechanisms of HA-cell/RBC fusion and FHA2-catalyzed cell/RBC fusion. Vesicle fusion induced by HA2 constructs also show pH dependence as well as reduction in fusion with the G1E and other mutations [19,21]. It is likely there are at least qualitative correlations between the mechanisms of HA-cell/RBC fusion and FHA2-catalyzed cell/RBC and vesicle fusion. Overall, these studies support the fusogenic nature of the trimer-of-hairpins structure including the significances of the SE and FP regions.

The Fig. 7 pictures of trimeric hairpin HA2 prior to fusion show two topologies in which the FP and TM domains are in (A) the same or (B) different membranes. The pictures may be relevant catalytic intermediates for: (1) vesicle/vesicle, (2) HA-cell/RBC; and (3) virus/endosome fusion with the TM in the (2) HA-cell or (3) viral

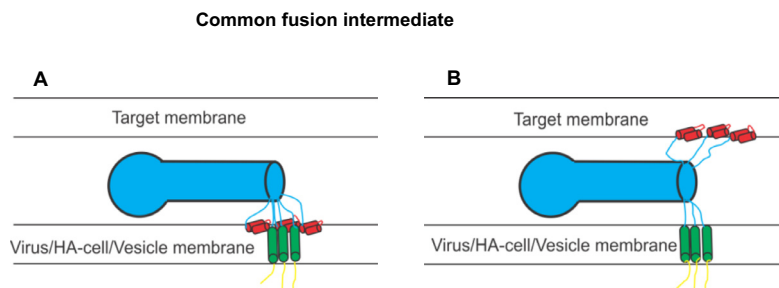


Fig. 7. Model of trimeric hairpin HA2 prior to fusion with the FP and TM regions in (A) the same membrane or (B) different membranes. The two membranes would correspond to: (1) two vesicles; (2) HA-cell and RBC; or (3) virus and endosome. For cases (2) and (3), the TM is respectively in the HA-cell and the viral membrane. The color coding is the same as Fig. 1 with FP (red), SE (blue), TM (green), and Endo (yellow). A single HA2 trimer is shown with structural elements: FP, helix-(tight-turn)-helix; SE, trimer-of-hairpins; and TM, helix. For either fusion type at $\text{pH} \approx 5$, the SE binds to both membranes in part because of attractive electrostatic energy between the positively-charged protein and negatively-charged membrane. The resultant membrane apposition and membrane perturbation aid catalysis of the subsequent membrane fusion. (For interpretation of the references to color in this figure legend, the reader is referred to the web version of this article.)

membrane. To our knowledge, there aren't yet data to distinguish between these topologies for any of these three cases. It is also possible that there is a distribution of FP's between the two membranes. For any FP/TM topology, virus/endosome fusion may be efficient because of the high virus/endosome collision rate in the restricted volume of the endosome.

Virus/vesicle and HA-cell/RBC fusion are greatly reduced when preceded by ~ 5 min low-pH pre-incubation without target membrane [21]. This reduction is often ascribed to insertion of the FP in the same membrane as the TM and it is therefore inferred that successful fusion requires FP insertion in the different (target) membrane. However, Fig. 6 in the present paper shows little vesicle fusion for times ≥ 10 s following protein addition. The absence of cell-cell fusion with pre-incubation for 5 min may therefore be due to intrinsic loss of protein activity rather than initial insertion of the FP in the same membrane as the TM.

For HA2-catalyzed vesicle fusion, the inter-vesicle collision rate is $\sim 10 \text{ s}^{-1}$ and the fusion rate is $\sim 0.2 \text{ s}^{-1}$ so there are ~ 50 collisions prior to fusion. This may result in FP's and TM's in different vesicles prior to fusion. Alternatively, they could plausibly insert in the same vesicle during the initial HA2/vesicle binding.

4.7. HIV vs influenza fusion

HIV fusion with the plasma membrane and influenza virus fusion with the endosome membrane are respectively catalyzed by the gp41 and HA2 proteins which are non-homologous in sequence but have similar final hairpin structures of the SE. Successful infection by HIV requires nucleocapsid release in the interior of the cell body with which the virus fuses, whereas infection by influenza requires release to the exterior of the body (endosome). Monomer species exist for both gp41 and HA2 proteins and may be functionally important because folding of the individual protein monomers to the final hairpin state is topologically more straightforward than folding of trimers [36,41–44]. The monomer is dominant for gp41 at pH 3–4 whereas the trimer is dominant for HA2 at pH 7.4 (Fig. 5). Hexamers containing the folded gp41 ectodomain are also observed and correlate with observation of HA2 oligomers larger than the trimer under some conditions [41,45]. Both gp41 and HA2 typically aggregate at their respective fusion pH's of ~ 7 and ~ 5 which may correlate to previous detection of multiple trimers for both proteins at the fusion site [46–49]. For HA2, the SE hairpin trimer has $T_m \approx 85^\circ \text{C}$ whereas the corresponding monomer hairpin SE of HIV gp41 has $T_m \approx 110^\circ \text{C}$ [50]. In addition, the HA2 T_m is higher with inclusion of the FP and/or TM. To our knowledge, there isn't evidence yet for this effect in monomer gp41.

Like HA2, vesicle fusion induced by gp41 is also enhanced by attractive protein/vesicle electrostatic energy [41,51,52].

Interestingly, fusion extent for gp41 is inversely-dependent on the magnitude of vesicle charge which probably reflects the effect of inter-vesicle electrostatic repulsion. For both proteins, the hairpin SE makes an important contribution to fusion with moderate enhancement with inclusion of the FP in the construct.

5. Conclusions

Full-length influenza virus hemagglutinin II membrane fusion protein as well as shorter constructs have been expressed and purified in mg quantities. The constructs typically adopt a folded trimer-of-hairpins structure in detergent and the full-length protein is hyperthermostable. The proteins induce vesicle fusion with significant contributions from the soluble ectodomain and fusion peptide and little contribution from the TM domain. The present as well as previous studies support a role for the final hairpin structure in catalysis of fusion between the viral and endosomal membranes.

Funding source

NIH R01 AI047153.

Acknowledgment

Dr. Dilini Ratnayake, Dr. A. Daniel Jones, and Mr. Douglas Whitten are acknowledged for providing guidance in the experimental design and analysis. Dr. Lisa Lapidus and Dr. Babak Borhan are acknowledged for use of the fluorescence and circular dichroism spectrometers in their laboratories. Mass spectra were obtained at the Mass Spectrometry and Proteomics facilities at Michigan State University.

Appendix A. Supplementary data

Supplementary data associated with this article can be found, in the online version, at <http://dx.doi.org/10.1016/j.pep.2015.08.021>.

References

- [1] J.M. White, S.E. Delos, M. Brecher, K. Schornberg, Structures and mechanisms of viral membrane fusion proteins: multiple variations on a common theme, *Crit. Rev. Biochem. Mol. Biol.* 43 (2008) 189–219.
- [2] M. Lakadamyali, M.J. Rust, H.P. Babcock, X.W. Zhuang, Visualizing infection of individual influenza viruses, *Proc. Natl. Acad. Sci. U.S.A.* 100 (2003) 9280–9285.
- [3] J. Gruenberg, Lipids in endocytic membrane transport and sorting, *Curr. Opin. Cell Biol.* 15 (2003) 382–388.
- [4] J. Gruenberg, Viruses and endosome membrane dynamics, *Curr. Opin. Cell Biol.* 21 (2009) 582–588.

- [5] I. Le Blanc, P.P. Luyet, V. Pons, C. Ferguson, N. Emans, A. Petiot, N. Mayran, N. Demaurex, J. Faure, R. Sadoul, R.G. Parton, J. Gruenberg, Endosome-to-cytosol transport of viral nucleocapsids, *Nat. Cell Biol.* 7 (2005) 653–664.
- [6] P. Durrer, C. Galli, S. Hoenke, C. Corti, R. Gluck, T. Vorherr, J. Brunner, H α -induced membrane insertion of influenza virus hemagglutinin involves the HA2 amino-terminal fusion peptide but not the coiled coil region, *J. Biol. Chem.* 271 (1996) 13417–13421.
- [7] G.W. Kemble, T. Danieli, J.M. White, Lipid-anchored influenza hemagglutinin promotes hemifusion, not complete fusion, *Cell* 76 (1994) 383–391.
- [8] T. Shangguan, D. Alford, J. Bentz, Influenza-virus-liposome lipid mixing is leaky and largely insensitive to the material properties of the target membrane, *Biochemistry* 35 (1996) 4956–4965.
- [9] H.E. Park, J.A. Gruenke, J.M. White, Leash in the groove mechanism of membrane fusion, *Nat. Struct. Biol.* 10 (2003) 1048–1053.
- [10] E. Borrego-Diaz, M.E. Peebles, R.M. Markosyan, G.B. Melikyan, F.S. Cohen, Completion of trimeric hairpin formation of influenza virus hemagglutinin promotes fusion pore opening and enlargement, *Virology* 316 (2003) 234–244.
- [11] C. Grewe, A. Beck, H.R. Gelderblom, HIV: early virus-cell interactions, *J. AIDS* 3 (1990) 965–974.
- [12] E. Nobusawa, T. Aoyama, H. Kato, Y. Suzuki, Y. Tateno, K. Nakajima, Comparison of complete amino acid sequences and receptor binding properties among 13 serotypes of hemagglutinins of influenza A viruses, *Virology* 182 (1991) 475–485.
- [13] S.R. Durell, I. Martin, J.M. Ruyschaert, Y. Shai, R. Blumenthal, What studies of fusion peptides tell us about viral envelope glycoprotein-mediated membrane fusion, *Mol. Membr. Biol.* 14 (1997) 97–112.
- [14] H. Qiao, R.T. Armstrong, G.B. Melikyan, F.S. Cohen, J.M. White, A specific point mutant at position 1 of the influenza hemagglutinin fusion peptide displays a hemifusion phenotype, *Mol. Biol. Cell* 10 (1999) 2759–2769.
- [15] R.T. Armstrong, A.S. Kushnir, J.M. White, The transmembrane domain of influenza hemagglutinin exhibits a stringent length requirement to support the hemifusion to fusion transition, *J. Cell Biol.* 151 (2000) 425–437.
- [16] B. Apellaniz, N. Huarte, E. Largo, J.L. Nieva, The three lives of viral fusion peptides, *Chem. Phys. Lipids* 181 (2014) 40–55.
- [17] S.A. Wharton, S.R. Martin, R.W.H. Ruigrok, J.J. Skehel, D.C. Wiley, Membrane-fusion by peptide analogs of influenza-virus hemagglutinin, *J. Gen. Virol.* 69 (1988) 1847–1857.
- [18] R.F. Epand, J.C. Macosko, C.J. Russell, Y.K. Shin, R.M. Epand, The ectodomain of HA2 of influenza virus promotes rapid pH dependent membrane fusion, *J. Mol. Biol.* 286 (1999) 489–503.
- [19] D.L. LeDuc, Y.K. Shin, R.F. Epand, R.M. Epand, Factors determining vesicular lipid mixing induced by shortened constructs of influenza hemagglutinin, *Biochemistry* 39 (2000) 2733–2739.
- [20] J. Curtis-Fisk, C. Preston, Z.X. Zheng, R.M. Worden, D.P. Weliky, Solid-state NMR structural measurements on the membrane-associated influenza fusion protein ectodomain, *J. Am. Chem. Soc.* 129 (2007) 11320–11321.
- [21] C.S. Kim, R.F. Epand, E. Leikina, R.M. Epand, L.V. Chernomordik, The final conformation of the complete ectodomain of the HA2 subunit of influenza hemagglutinin can by itself drive low pH-dependent fusion, *J. Biol. Chem.* 286 (2011) 13226–13234.
- [22] I.A. Wilson, J.J. Skehel, D.C. Wiley, Structure of the haemagglutinin membrane glycoprotein of influenza virus at 3 Å resolution, *Nature* 289 (1981) 366–373.
- [23] J. Chen, J.J. Skehel, D.C. Wiley, N- and C-terminal residues combine in the fusion-pH influenza hemagglutinin HA $_2$ subunit to form an N cap that terminates the triple-stranded coiled coil, *Proc. Natl. Acad. Sci. U.S.A.* 96 (1999) 8967–8972.
- [24] X. Han, J.H. Bushweller, D.S. Cafiso, L.K. Tamm, Membrane structure and fusion-triggering conformational change of the fusion domain from influenza hemagglutinin, *Nat. Struct. Biol.* 8 (2001) 715–720.
- [25] J.L. Lorieau, J.M. Louis, A. Bax, The complete influenza hemagglutinin fusion domain adopts a tight helical hairpin arrangement at the lipid:water interface, *Proc. Natl. Acad. Sci. U.S.A.* 107 (2010) 11341–11346.
- [26] T.P. Du, L. Jiang, M.L. Liu, NMR structures of fusion peptide from influenza hemagglutinin H3 subtype and its mutants, *J. Peptide Sci.* 20 (2014) 292–297.
- [27] U. Ghosh, L. Xie, L.H. Jia, S. Liang, D.P. Weliky, Closed and semiclosed structures in membrane vs closed and open structures in detergent for the influenza virus hemagglutinin fusion peptide and correlation of hydrophobic surface area with fusion catalysis, *J. Am. Chem. Soc.* 115 (2015) 7548–7551.
- [28] Y. Sun, D.P. Weliky, ^{13}C - ^{15}N Correlation spectroscopy of membrane-associated Influenza virus fusion peptide strongly supports a helix-turn-helix motif and two turn conformations, *J. Am. Chem. Soc.* 131 (2009) 13228–13229. PMID: 2772195.
- [29] U. Ghosh, L. Xie, D.P. Weliky, Detection of closed influenza virus hemagglutinin fusion peptide structures in membranes by backbone ^{13}C - ^{15}N rotational-echo double-resonance solid-state NMR, *J. Biomol. NMR* 55 (2013) 139–146.
- [30] S.E. Swalley, B.M. Baker, L.J. Calder, S.C. Harrison, J.J. Skehel, D.C. Wiley, Full-length influenza hemagglutinin HA $_2$ refolds into the trimeric low-pH-induced conformation, *Biochemistry* 43 (2004) 5902–5911.
- [31] J. Curtis-Fisk, R.M. Spencer, D.P. Weliky, Isotopically labeled expression in *E. coli*, purification, and refolding of the full ectodomain of the Influenza virus membrane fusion protein, *Protein Expression Purif.* 61 (2008) 212–219.
- [32] E.P. Vogel, D.P. Weliky, Quantitation of recombinant protein in whole cells and cell extracts via solid-state NMR spectroscopy, *Biochemistry* 52 (2013) 4285–4287.
- [33] E.P. Vogel, J. Curtis-Fisk, K.M. Young, D.P. Weliky, Solid-state nuclear magnetic resonance (NMR) spectroscopy of human immunodeficiency virus gp41 protein that includes the fusion peptide: NMR detection of recombinant Fgp41 in inclusion bodies in whole bacterial cells and structural characterization of purified and membrane-associated Fgp41, *Biochemistry* 50 (2011) 10013–10026.
- [34] X. Han, L.K. Tamm, A host-guest system to study structure-function relationships of membrane fusion peptides, *Proc. Natl. Acad. Sci. U.S.A.* 97 (2000) 13097–13102.
- [35] J. Chen, J.J. Skehel, D.C. Wiley, A polar octapeptide fused to the N-terminal fusion peptide solubilizes the influenza virus HA(2) subunit ectodomain, *Biochemistry* 37 (1998) 13643–13649.
- [36] N.A. Lakomek, J.D. Kaufman, S.J. Stahl, J.M. Louis, A. Grishaev, P.T. Wingfield, A. Bax, Internal dynamics of the homotrimeric HIV-1 viral coat protein gp41 on multiple time scales, *Angew. Chem. Int. Ed.* 52 (2013) 3911–3915.
- [37] T. Kobayashi, M.H. Beuchat, J. Chevallier, A. Makino, N. Mayran, J.M. Escola, C. Lebrand, P. Cosson, T. Kobayashi, J. Gruenberg, Separation and characterization of late endosomal membrane domains, *J. Biol. Chem.* 277 (2002) 32157–32164.
- [38] W. Mobius, E. van Donselaar, Y. Ohno-Iwashita, Y. Shimada, H.F.G. Heijnen, J. W. Slot, H.J. Geuze, Recycling compartments and the internal vesicles of multivesicular bodies harbor most of the cholesterol found in the endocytic pathway, *Traffic* 4 (2003) 222–231.
- [39] C.M. Carr, P.S. Kim, A spring-loaded mechanism for the conformational change of influenza hemagglutinin, *Cell* 73 (1993) 823–832.
- [40] E. Leikina, D.L. LeDuc, J.C. Macosko, R. Epand, Y.K. Shin, L.V. Chernomordik, The 1–127 HA2 construct of influenza virus hemagglutinin induces cell-cell hemifusion, *Biochemistry* 40 (2001) 8378–8386.
- [41] K. Banerjee, D.P. Weliky, Folded monomers and hexamers of the ectodomain of the HIV gp41 membrane fusion protein: Potential roles in fusion and synergy between the fusion peptide, hairpin, and membrane-proximal external region, *Biochemistry* 53 (2014) 7184–7198.
- [42] J. Roche, J.M. Louis, A. Grishaev, J.F. Ying, A. Bax, Dissociation of the trimeric gp41 ectodomain at the lipid-water interface suggests an active role in HIV-1 Env-mediated membrane fusion, *Proc. Natl. Acad. Sci. U.S.A.* 111 (2014) 3425–3430.
- [43] M. Caffrey, J. Kaufman, S. Stahl, P. Wingfield, A.M. Gronenborn, G.M. Clore, Monomer-trimer equilibrium of the ectodomain of SIV gp41: insight into the mechanism of peptide inhibition of HIV infection, *Protein Sci.* 8 (1999) 1904–1907.
- [44] Z. Dai, Y.S. Tao, N.N. Liu, M.D. Brenowitz, M.E. Girvin, J.R. Lai, Conditional trimerization and lytic activity of HIV-1 gp41 variants containing the membrane-associated segments, *Biochemistry* 54 (2015) 1589–1599.
- [45] G.F. Gao, L. Wiczorek, K.K. Peachman, V.R. Polonis, C.R. Alving, M. Rao, V.B. Rao, Designing a soluble near full-length HIV-1 gp41 trimer, *J. Biol. Chem.* 288 (2013) 234–246.
- [46] E.O. Freed, E.L. Delwart, G.L. Buchschacher Jr., A.T. Panganiban, A mutation in the human immunodeficiency virus type 1 transmembrane glycoprotein gp41 dominantly interferes with fusion and infectivity, *Proc. Natl. Acad. Sci. U.S.A.* 89 (1992) 70–74.
- [47] J. Bentz, Minimal aggregate size and minimal fusion unit for the first fusion pore of influenza hemagglutinin-mediated membrane fusion, *Biophys. J.* 78 (2000) 227–245.
- [48] R. Sougrat, A. Bartesaghi, J.D. Lifson, A.E. Bennett, J.W. Bess, D.J. Zabransky, S. Subramaniam, Electron tomography of the contact between T cells and SIV/HIV-1: implications for viral entry, *PLoS Pathog.* 3 (2007) 570–581.
- [49] C. Magnus, P. Rusert, S. Bonhoeffer, A. Trkola, R.R. Regoes, Estimating the stoichiometry of Human Immunodeficiency Virus entry, *J. Virol.* 83 (2009) 1523–1531.
- [50] K. Sackett, M.J. Nethercott, R.F. Epand, R.M. Epand, D.R. Kindra, Y. Shai, D.P. Weliky, Comparative analysis of membrane-associated fusion peptide secondary structure and lipid mixing function of HIV gp41 constructs that model the early pre-hairpin intermediate and final hairpin conformations, *J. Mol. Biol.* 397 (2010) 301–315.
- [51] K. Sackett, A. TerBush, D.P. Weliky, HIV gp41 six-helix bundle constructs induce rapid vesicle fusion at pH 3.5 and little fusion at pH 7.0: understanding pH dependence of protein aggregation, membrane binding, and electrostatics, and implications for HIV-host cell fusion, *Eur. Biophys. J.* 40 (2011) 489–502.
- [52] P.U. Ratnayake, K. Sackett, M.J. Nethercott, D.P. Weliky, pH-dependent vesicle fusion induced by the ectodomain of the human immunodeficiency virus membrane fusion protein gp41: two kinetically distinct processes and fully-membrane-associated gp41 with predominant beta sheet fusion peptide conformation, *Biochim. Biophys. Acta* 1848 (2015) 289–298.

Supplementary Material for “Full-Length Trimeric Influenza Virus Hemagglutinin II Membrane Fusion Protein and Shorter Constructs Lacking the Fusion Peptide or Transmembrane Domain: Hyperthermostability of the Full-Length Protein and the Soluble Ectodomain and Fusion Peptide Make Significant Contributions to Fusion of Membrane Vesicles” by Punsisi U. Ratnayake, Sweta S. Komanduru, E. A. Prabodha Ekanayaka, and David P. Weliky

1. *Material sources*

Molecular biology and Cells: pUC57-Kan plasmids, Genscript; Restriction enzymes – New England Bio Labs; Competent *E. coli* cells – Novagen, Super Signal West Pico chemiluminescent substrate – Thermo Scientific.

Detergents and Lipids: DM – Affymetrix; *N*-NBD-DPPE, *N*-Rh-DPPE, DOTAP, POPC, and POPG – Avanti Polar Lipids; *N*-lauroylsarcosine, Biomedicals; Cholesterol, Fisher Scientific. Most other reagents were purchased from Sigma–Aldrich.

HA2: residues 1-221 with G₆LEH₆ non-native C-terminal tag

```
1  GLFGAIAGFIENGWEGMIDGWYGF20FRHQNSEGTGQAADLKSTQAAIDQINGKLN61RVI121EKTN  
61  EK121FHQIEKEFSEVEGRIQDLEKYVEDTKIDLWSYNAELLVALENQHTIDLT181DSEM181NKLF181E  
121  KTRRQLRENAEEMGNGSF181KIYHKADNAAIESIRNGTYDHDVYRDEALNNRFQIKGVELKS  
181  GYKDWILWISFAISAFLLAVVLLGFMWAAQ181RG181NI181RANIAI181GGGGGGLEHHHHHH
```

FHA2: residues 1-185 with LEH₆ non-native C-terminal tag

```
1  GLFGAIAGFIENGWEGMIDGWYGF20FRHQNSEGTGQAADLKSTQAAIDQINGKLN61RVI121EKTN  
61  EK121FHQIEKEFSEVEGRIQDLEKYVEDTKIDLWSYNAELLVALENQHTIDLT181DSEM181NKLF181E  
121  KTRRQLRENAEEMGNGSF181KIYHKADNAAIESIRNGTYDHDVYRDEALNNRFQIKGVELKS  
181  GYKDWLEHHHHHH
```

SHA2: residues 20-185 with G20C mutation and LEH₆ non-native C-terminal tag

```
20  CWYGF20FRHQNSEGTGQAADLKSTQAAIDQINGKLN61RVI121EKTN  
61  EK121FHQIEKEFSEVEGRIQDLEKYVEDTKIDLWSYNAELLVALENQHTIDLT181DSEM181NKLF181E  
121  KTRRQLRENAEEMGNGSF181KIYHKADNAAIESIRNGTYDHDVYRDEALNNRFQIKGVELKS  
181  GYKDWLEHHHHHH
```

SHA2-TM₂₆: residues 20-211 with G20C mutation and G₆LEH₆ non-native C-terminal tag

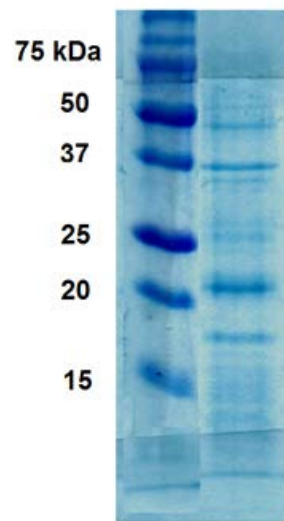
```
20  CWYGF20FRHQNSEGTGQAADLKSTQAAIDQINGKLN61RVI121EKTN  
61  EK121FHQIEKEFSEVEGRIQDLEKYVEDTKIDLWSYNAELLVALENQHTIDLT181DSEM181NKLF181E  
121  KTRRQLRENAEEMGNGSF181KIYHKADNAAIESIRNGTYDHDVYRDEALNNRFQIKGVELKS  
181  GYKDWILWISFAISAFLLAVVLLGFMWAAQ181GGGGGGLEHHHHHH
```

Figure S1. Sequences of some of the HA2 constructs with color coding matching Fig. 1A. The non-native C-terminal regions are shown in black and include a H₆ tag for affinity chromatography. For constructs that include the TM region, G₆ is added as a flexible region to increase H₆ exposure during chromatography.

1 ggtctggtcgggtgctatcgctggctttattgaaaacggttgggaaggcatgatcgacggc
61 tggtagcggttttcgccatcaaaactcagaaggcaccggtcaggcggcggatctgaaaagc
121 acgcaggcagctattgaccaaatacaacggcaaactgaatcgtgtgatcgaaaaaccaac
181 gaaaaattccatcagatcgaaaaagaattttctgaagtcgaaggcgcattcaagatctg
241 gaaaaatatgtggaagatacgaaaaatcgacctgtggtcatacaacgcgggaactgctggtt
301 gccctggaaaatcagcacaccattgatctgacggactcggaaatgaacaaactgttcgaa
361 aaaaccgctcgccaactgcgtgaaaacgcagaagaaatgggcaacggtagtttcaaaatc
421 taccataaagctgataacgcggccattgaatccatccgcaatggcacgtatgatcacgac
481 gtttaccgctgacgaagcgtgaacaatcgctttcagattaaaggcgtcgaactgaaatcc
541 ggttacaaagattggattctgtggatcagctttgcaatttctgctttcctgctggccgtg
601 gttctgctgggtttcatcatgtgggcggcgcagcgtggcaacattcgtgcaaacatcgca
661 atcgggtggcgggtggcggcggcctcgagcaccaccaccaccaccac

Figure S2. DNA sequence that codes for the amino acid sequence of HA2 displayed in Fig. S1.

A Solubilization with urea



B Solubilization with SRC

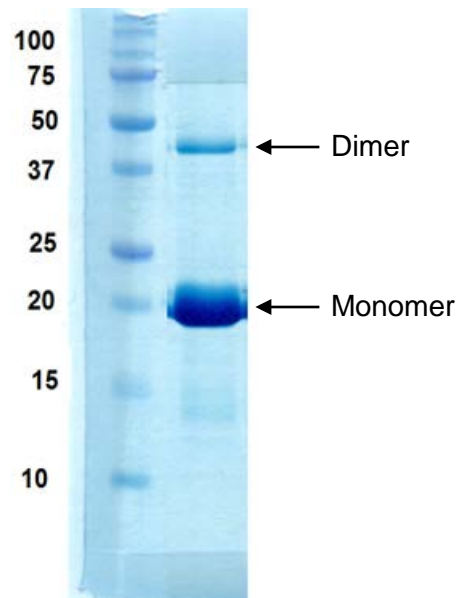
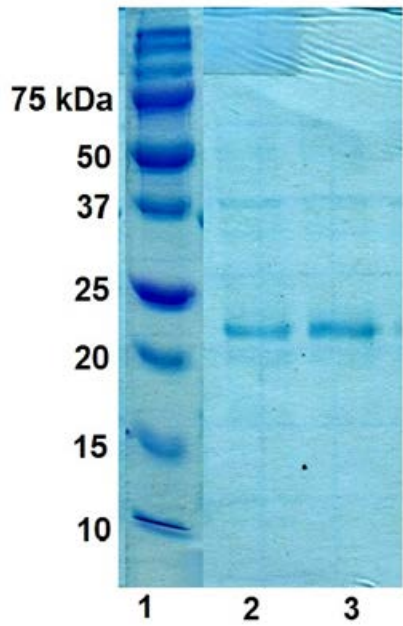


Figure S3. SDS-PAGE of purification eluents for SHA2-TM₂₁. The cells were first lysed in PBS followed by centrifugation to separate the insoluble material enriched in RP from the soluble fraction enriched in bacterial proteins. The procedure was repeated three times and the pellet was then solubilized with buffer containing either (A) 8 M urea; or (B) 0.5% (w/v) SRC with subsequent Co²⁺ affinity purification.

A SHA2-TM₂₆ with LEH₆ tag



B SHA2-TM₂₆ with G₆LEH₆ tag

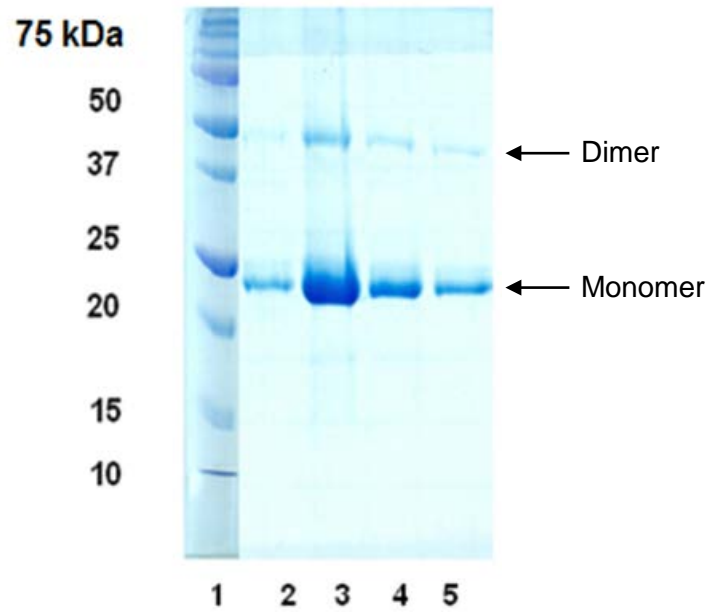
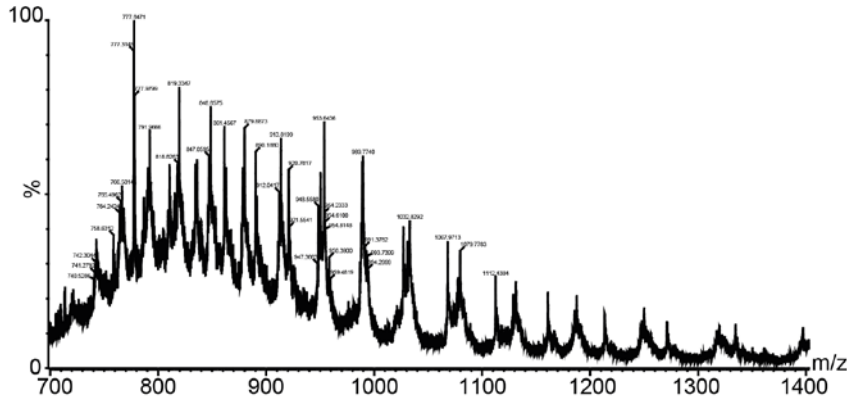
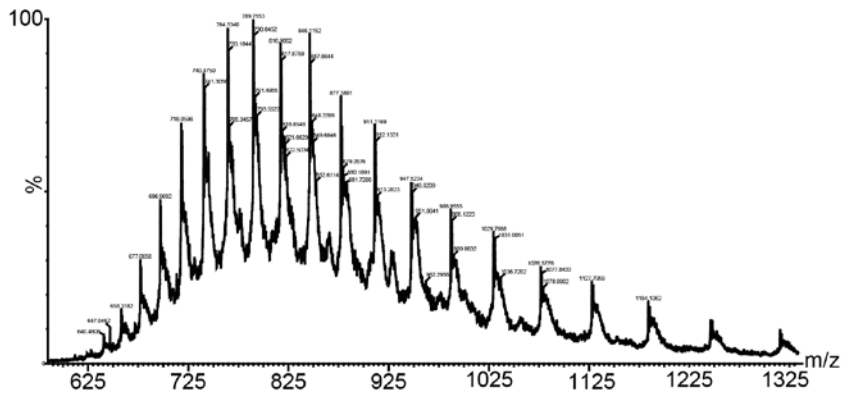


Figure S4. SDS-PAGE of purification eluents for SHA2-TM₂₆ with either a (A) LEH₆ or (B) G₆LEH₆ C-terminal tag. Sequential 0.5 mL elutions are shown in (A) lanes 2 and 3 and (B) lanes 2-5.

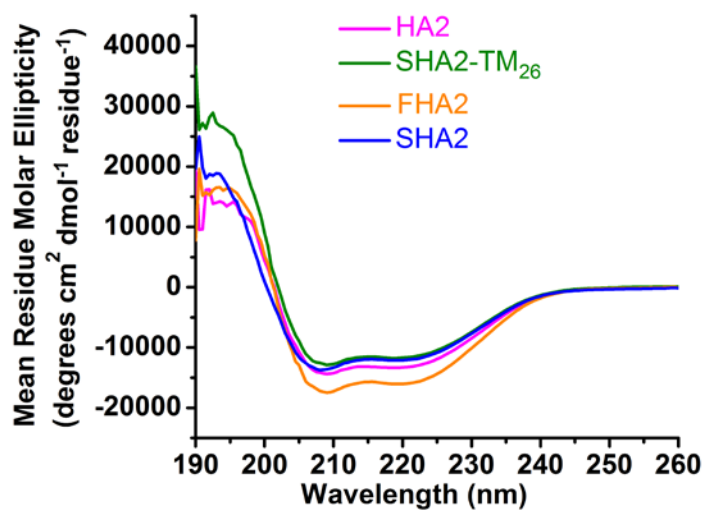
HA2



SHA2-TM₂₆



A Circular dichroism spectra at pH 9.0 and ambient temperature



B Circular dichroism spectra of FHA2 at pH 7.4 and ambient temperature

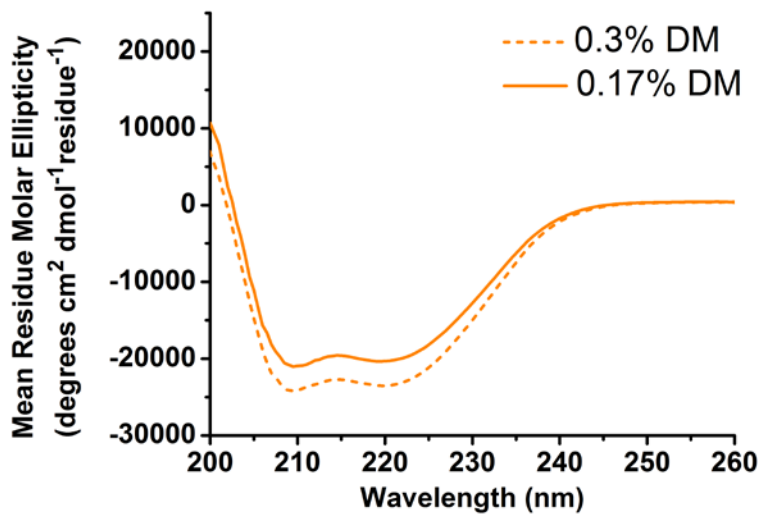
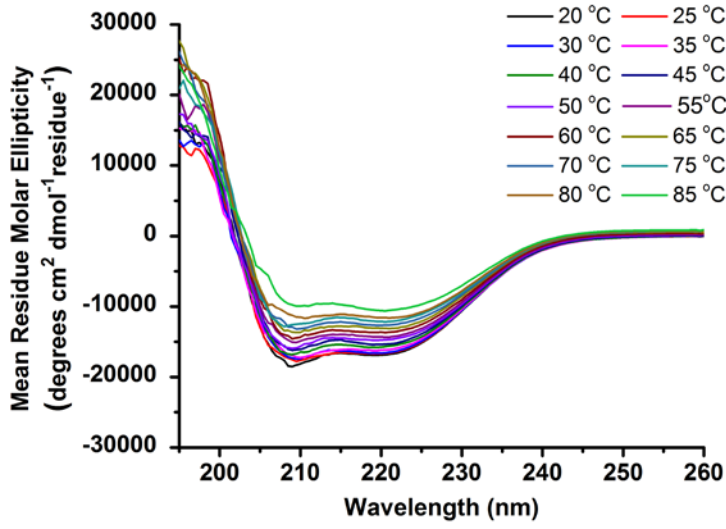
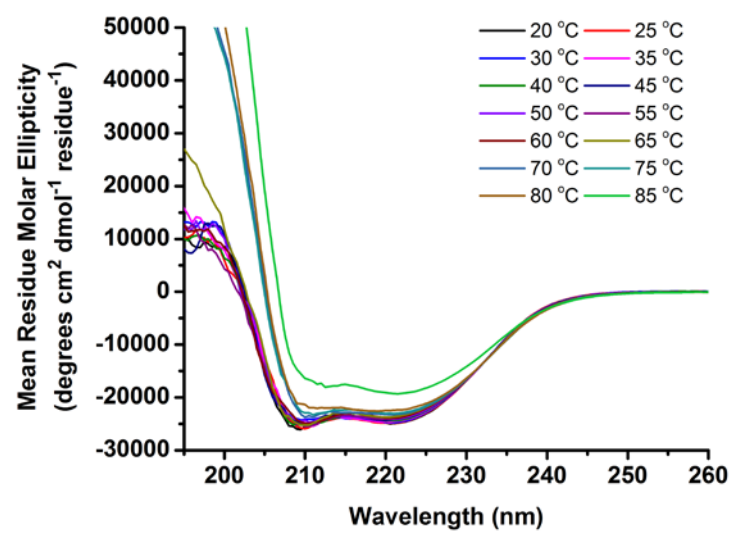


Figure S6

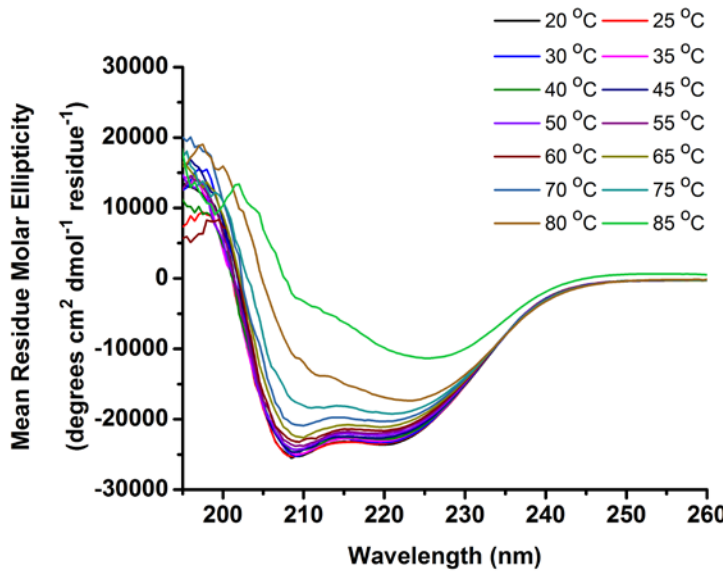
HA2



SHA2-TM₂₆



FHA2



SHA2

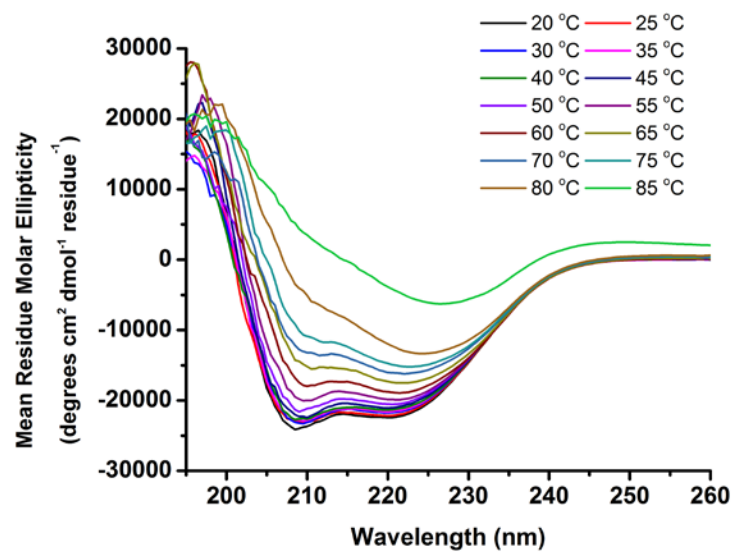


Figure S7. Circular dichroism spectra at pH 7.4 in 0.17% DM detergent.

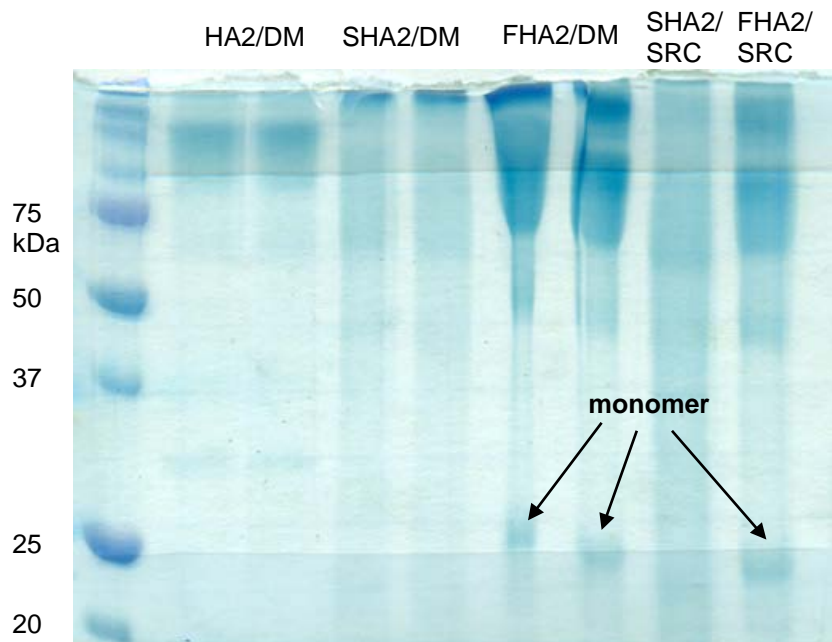
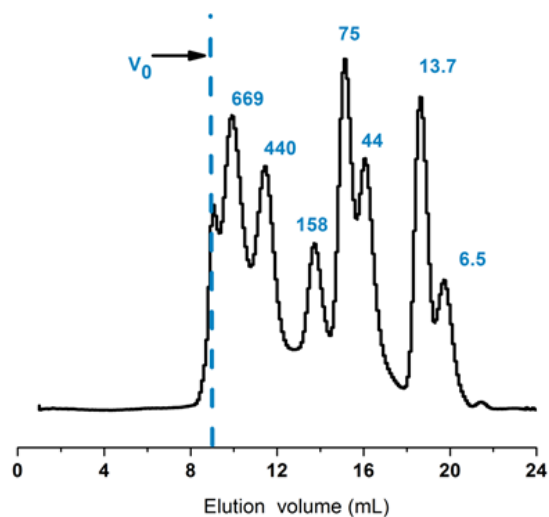


Figure S8. SDS-PAGE of protein after one hour of chemical cross-linking. The faint marked bands are assigned as protein monomer. This is a 15% gel.

A SEC of MW standards



B SEC analysis

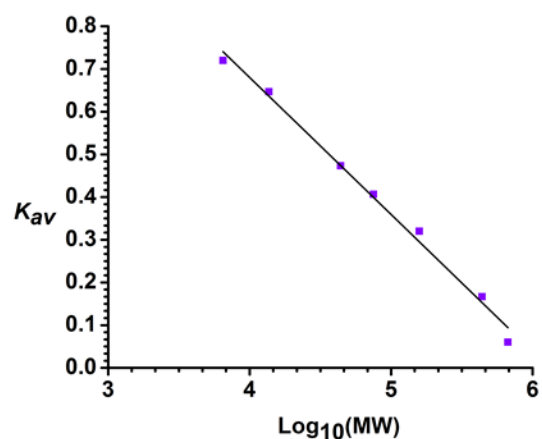


Figure S9. SEC (A) plot and (B) analysis of MW standards. The SEC was done with a Superdex 200 column with A_{280} detection. For each standard, K_{av} was calculated as $[(V_e - V_o)/(V_c - V_o)]$ using $V_e \equiv$ elution volume of the standard, $V_o \equiv$ column void volume, and $V_c \equiv$ column volume. The standards include the thyroglobulin (669 kDa), ferritin (440 kDa), aldolase (158 kDa), conalbumin (75 kDa), Ovalbumin (44 kDa), carbonic anhydrase (29 kDa), ribonuclease A (13.7 kDa), and aprotinin (6.5 kDa). V_o corresponded to blue dextran with MW = 2 MDa.

SEC in 0.17% DM at pH 7.4

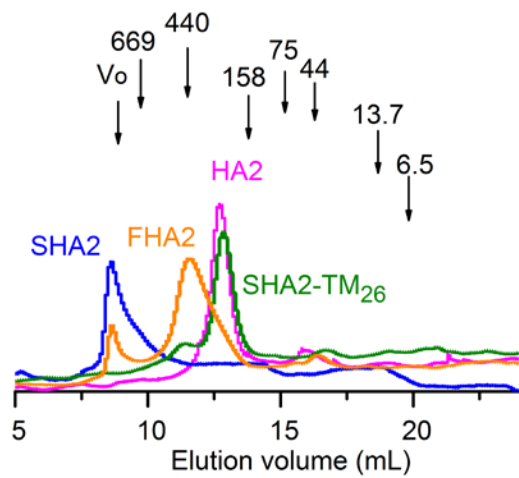


Figure S10

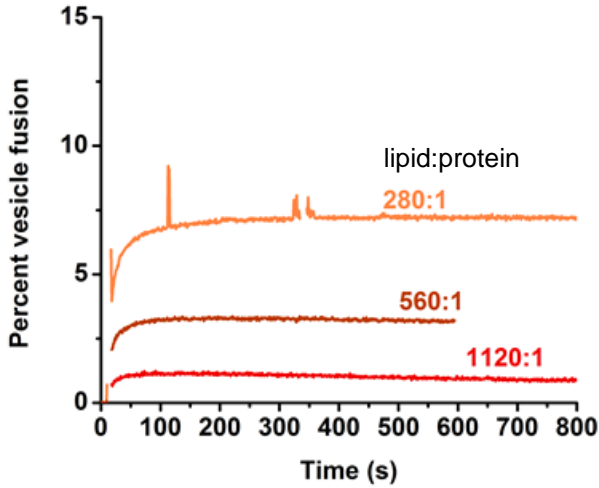
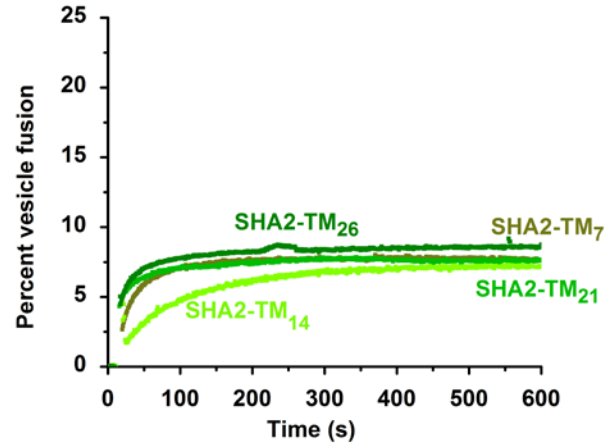
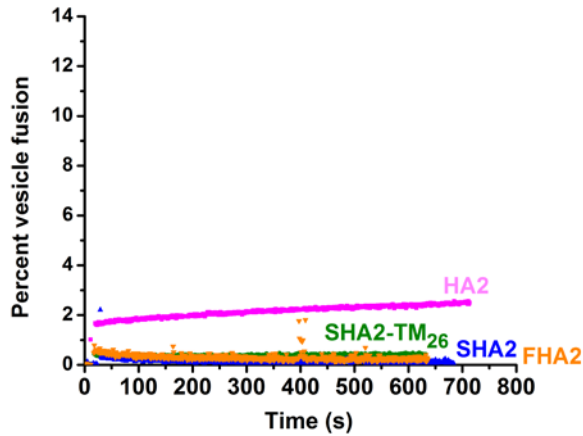
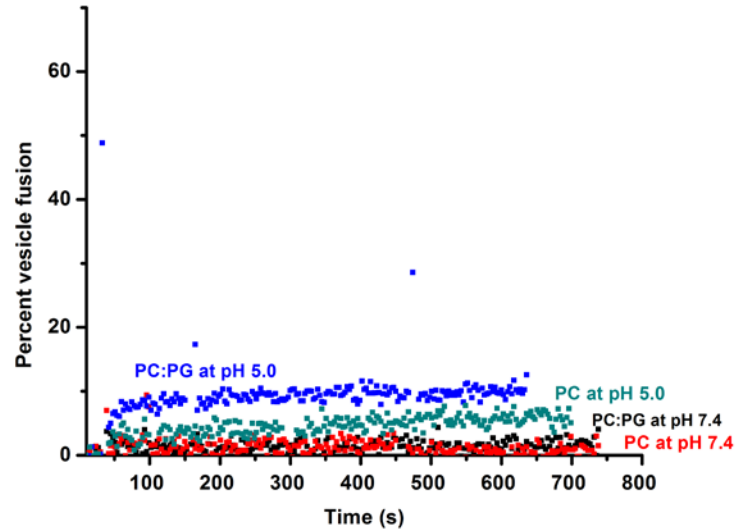
A Dose response for SHA2 at pH 5.0**B** Fusion by different SHA2-TM at pH 5.0**C** Fusion at pH 7.4**D** HA2-induced fusion of neutral vs negatively-charged vesicles

Figure S11. (A-C) Protein-induced fusion of negatively-charged vesicles including (A) dose response for SHA2 at pH 5.0; (B) different SHA2-TM constructs at pH 5.0; and (C) data at pH 7.4. The vesicles contained POPC:POPG (4:1) and for panels B and C, the protein:lipid mole ratio = 1:280. (D) HA2-induced fusion for POPC-only and POPC:POPG (4:1) vesicles with protein:lipid = 1:140. Replicate assays consistently showed at least twice the fusion for PC:PG vesicles relative to PC-only vesicles at 50 s after protein addition. Because of instrument breakage, the (D) vesicle fusion assays were done with a different fluorimeter than the rest of the assays of this study. Because this fluorimeter had lower sensitivity, we needed to increase the integration and sampling times to 3 s.